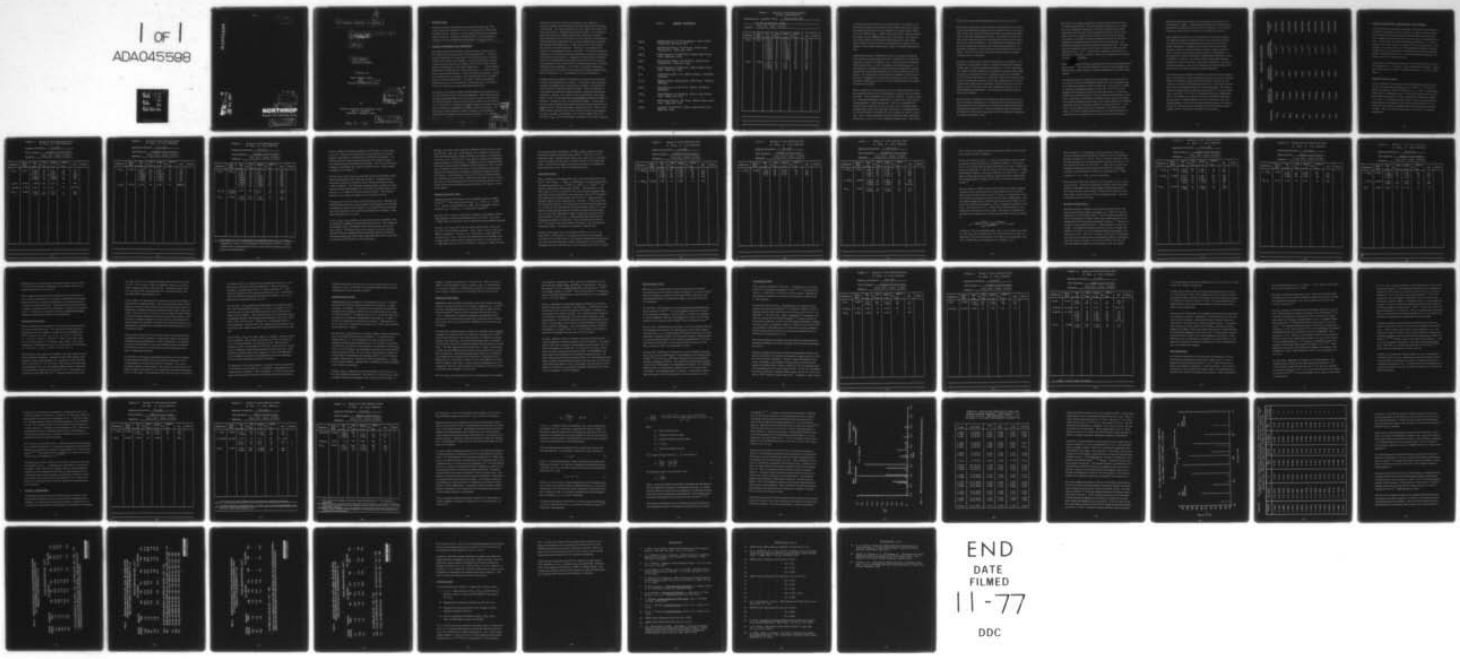
AD-A045 598 NORTHROP RESEARCH AND TECHNOLOGY CENTER HAWTHORNE CALIF F/G 11/3
OPTICAL COATINGS 2-6 MICRONS.(U)
SEP 77 P KRAATZ N00123-76-C-1321
NL

UNCLASSIFIED

1 OF 1
ADA045598



END
DATE FILMED
11-77
DDC

AD A045598

AD No.
DDC FILE COPY

DDC
RECEIVED
OCT 27 1977
A

NORTHROP

Research and Technology Center

DISTRIBUTION STATEMENT A
Approved for public release;
Distribution Unlimited

(19)

(6) OPTICAL COATINGS 2-6 MICRONS.

(9) Technical Report. Jan - Jun 77

(11) September 1977

(12) 63p.

(10) P. Kraatz
Principal Investigator

Prepared For

Naval Weapons Center

(15) Contract No. N00123-76-C-1321

DDC
RECEIVED
OCT 27 1977
A

By

Northrop Research and Technology Center
3401 W. Broadway
Hawthorne, California 90250

DISTRIBUTION STATEMENT A
Approved for public release;
Distribution Unlimited

AD A047696

4B

1. INTRODUCTION

Progress during the second half-year (January through June, 1977) under Contract No. N00123-76-C-1321 is reported here. The report is divided into four sections covering coating materials and deposition, coating structure, orientation, and growth rates, coating properties (refractive indices and absorption coefficients), and future plans. The materials include sapphire; fluorides of lanthanum, lead, *

2. COATING MATERIALS AND DEPOSITION

Successful deposition of thin film coatings requires careful control of the evaporation technique and the associated parameters. Currently, thermal evaporation in a high vacuum is the technique that is most frequently used to deposit film coatings. Thermal evaporation in a high vacuum has been extensively developed, and two of the most common modes of evaporation are resistance heating and e[illegible]n-beam heating. Both modes of evaporation are widely used, and it is relatively easy to produce good optical coatings. In spite of this favorable aspect, results of investigations of the properties of evaporated films have not always shown the expected consistency. The cause of these discrepancies probably does not lie in the method of evaporation itself, but rather in the lack of control of the many experimental parameters.

The quality of the optical coating materials depends on the purity of the starting materials and the method of preparation. Since impurities can increase optical absorption as well as initiate a variety of macroscopic or structural defects, commercial materials of highest purity must be used. The purity is frequently given in percentage of the main material, up to 99.9999%; the remainder consisting of unknown impurities. Although this number indicates ultrapure material, it still contains a great number of impurity atoms per cubic centimeter. It is, therefore,

* magnesium, strontium, thorium; silicon oxide, magnesium oxide; zinc sulfide, zinc selenide; lanthanum oxyfluoride.

per Litton file
DISTRIBUTION/AVAILABILITY CODES
Dist. AVAIL. and/or SPECIAL
A

necessary to know the kind and concentration of all impurities. A variety of methods exist for the detection and determination of impurity concentration. The most important are x-ray, optical absorption, and mass spectroscopy. Knowing the impurities present, it is essential to determine which ones actually influence the respective properties. These impurities must be removed or at least reduced in concentration. Coating materials of desired purity are only available when a material has attained broad application. In most cases, it has to be purified; this is quite an involved operation. Drying is very essential if the material is contaminated by water in any form. The effects of absorbed moisture are so pronounced that they completely mask the normal aging and the basic loss mechanism. Adsorbed or trapped water or hydroxyl ions can be eliminated by drying under vacuum and slowly increasing the temperature to the level at which the loosely bound water is removed by diffusion and evaporation. True oxide or hydroxide compounds in solid form are not removable by this means, but require chemical reaction in some form, (i.e., scavenging by a reactive atmosphere).

Coating materials employed in the program are listed and identified as to source and nominal purity in Table 1. In all cases, these materials represent the highest purity commercially available. No attempt was made to further purify any of these materials. All were subjected to x-ray diffraction analysis to determine phase composition and identify impurities. Results were reported in the first quarterly report (September, 1976), for all materials except Lanthanum Fluoride and Silicon Monoxide. Results for LaF_3 are presented in Table 2. In this table, the first column identifies the material and phase determinable from the diffraction line. The second column, headed "Card Ref." refers to the ASTM Powder Diffraction File Card on which the data for the material or phase in question are tabulated. The columns headed "Obs. d(Å)" and "Obs. I/I_{100}" give the interplanar spacing in Å and relative intensity

TABLE 1. COATING MATERIALS

Al_2O_3	Random Chunks of UV-Grade Sapphire, Union Carbide Corporation, San Diego, Calif.
LaF_3	Hot-Pressed Tablets, 99.9% Purity, Balzers High Vacuum Corp., Santa, Ana, Calif.
MgF_2	Fused Granules, 99.99% Purity, Balzers High Vacuum Corp., Santa Ana, Calif.
MgO	Hot-Pressed Tablets, 99.95% Purity, Balzers High Vacuum Corp., Santa Ana, Calif.
PbF_2	Fused Granules, 99.99% Purity, Balzers High Vacuum Corp., Santa Ana, Calif.
SiO	Linde Select Grade, R. D. Mathis Company, Long Beach, California.
SrF_2	Random Chunks, Optical Grade, EMCO Sales, Anaheim, California.
ThF_4	Fused Granules, 99.9% Purity, CERAC, Milwaukee, Wisconsin.
ThF_4	Fused Granules, 99.9% Purity, Balzers, High Vacuum Corp., Santa, Ana, Calif.
ZnS	Hot-Pressed Tablets, 99% Purity, Balzers High Vacuum Corp., Santa Ana, Calif.
ZnSe	Granules, 99.99% Purity, Balzers High Vacuum Corp., Santa Ana, Calif.

TABLE 2 . Results of X-Ray Diffraction Study of LaF_3 Coating Material.

Material Source, Condition, Purity : Balzers Ch72-390/3 (99.9%) As Received, Ground.

Radiation : CuK_α 35 kV. 18 mA. Ni Filter

Material	Card Ref.	Obs d (Å)	Obs I/I_{100}	ASTM d (Å)	ASTM I/I_{100}	hkl	Notes
LaF_3	8-461	3.667	32	3.67	40	002	
		3.580	19	3.59	32	110	
		3.218	59	3.229	100	111	
		2.5615	07	2.569	11	112	
		2.0213	43	2.025	54	113	
		1.8024	27	1.8064	33	302	
		1.7477	27	1.7451	20	221	
		1.4455	08	1.4487	14	223	
		1.3346	19	1.3354	15	411	
		1.1872	14	1.1877	14	413	
LaOF	5-0470	3.348	100	3.35	100	101	
		2.905	22	2.90	25	110	
		2.0606	46	2.06	60	112	
		1.7634	22	1.76	22	103	

of diffraction peaks observed in the present study. To facilitate comparison and emphasize pecularities of the evaporant material, the Powder Diffraction File data are also tabulated in columns headed "ASTM d (Å)" and "ASTM I/I_{100}". Miller indices (hkl) of the respective diffracting planes are also tabulated when given on the cards. The main feature of this analysis worth noting is that diffraction lines for LaOF (which should be present only in trace amounts as an impurity) are as intense or more intense than those for LaF_3, the nominal coating material.

Although the intensity of diffracted x-rays is not simply proportional to the amount of a given phase present in a sample (due to losses from absorption, preferred orientation, etc.), such high relative intensities indicate that LaOF is a major constituent of the coating material. If this material is redeposited on substrates during evaporation, coating inhomogeneities and high absorptance in the mid-infrared would be expected. The redeposition of this material in addition to oxides and hydroxides of Lanthanam is in fact found in conjunction with a very high absorption coefficient at 3.8 μm, as will be demonstrated in successive sections of this report.

Silicon monoxide was also subjected to x-ray diffraction analysis, with the expectation that it would be amorphous to x-ray and show no diffraction peaks. This expectation was very nearly fulfilled. A single, broad, very weak diffraction peak attributable to α quartz (101) with a spacing of approximately 3.348Å was detected. This is not unexpected and should cause no particular concern for the 3.8 μm wavelength region. Although SiO_2 itself is not especially detrimental to coating absorption in the mid infrared, its tendency to act as a getter for water is a problem. Thus, a film consisting of SiO and redeposited SiO_2 could absorb heavily at 5.3 μm or 2.7 μm if it contained trapped water. This will be

discussed in connection with absorption results in a later section.

In the vacuum deposition of thin films by an evaporation process, knowledge of the substrate temperature and its control is often very important. In fact, the substrate temperature plays an especially important role for the whole condensation process. It controls the surface mobility of the condensing atoms or molecules and determines the degree of disorder of the growing film. Film adhesion and durability are improved by heating the substrates prior to and during deposition. Of paramount importance is the removal of adsorbed gases from the substrate. Thus water removal is one of the main reasons for heating substrates prior to deposition.

In practice a wide range of substrate temperatures is employed. The deposition of metal oxides requires substrate temperatures of approximately 300°C to obtain optimal film properties.[1] On the other hand, zinc sulfide should be deposited at a substrate temperature below 180°C to provide a compromise between reevaporation and film durability.[2] If a low substrate temperature is required to obtain a desired film property such as minimal scattering, and if this temperature is too low to remove water vapor from the substrate, then the substrate can be preheated to remove the water vapor and subsequently cooled to the required deposition temperature. Glow discharge cleaning can also be used in this situation.

Since the index of refraction of the films and film structure are a function of substrate temperature, it is important that both substrates and monitoring pieces be maintained at a uniform and constant temperature throughout the deposit cycle. A typical substrate heater is described by Mattauch[3] and the measurement and control of substrate temperature is discussed by Hanson, et al.[4]

The objective in vacuum evaporation is nearly always to deposit films to certain specifications. If the specification is primarily one of thickness, it is sufficient to determine when the accumulated deposit has reached the desired value so that the deposition process can be terminated. However, intensive film properties such as density, stress, crystallinity, and index of refraction depend on the rates at which the evaporant and residual gas molecules arrive at the substrate. It is therefore necessary to maintain specified evaporation rates. The influence of the deposition rates on the index of refraction of SiO has been studied by Hass, et. al.[5] A high rate of deposition corresponds to a high index of refraction, whereas, a slow rate of deposition corresponds to a low index of refraction.

Reviews of thickness and rate monitors have been given by Steckelmacher[6] and Behrndt.[7] The control of evaporation rate is a more complex task than thickness control because it requires adjustment of the source temperature.

All coating depositions required for this program were carried out in a commercial vacuum system (Balzers Model 710) which is equipped with an oil diffusion pump and a liquid nitrogen trap. This system is capable of routinely maintaining pressures of the order of 10^{-6} Torr and is equipped with a substrate heater and a thin film monitor to control deposition rate and film thickness. Proper control of the thickness of each layer is afforded by observing the reflectance at the control wavelength of a suitably positioned monitor plate in the coating chamber and stopping deposition when the reflectance reaches a predetermined level. In all cases, care is taken to ensure the uniformity of the thickness of the layers. In order to obtain uniform layers, the window substrates are rotated above the evaporation source during the deposition process.

Deposition parameters utilized in this program are summarized for each material in Table 3. Electron beam heating was employed in the evaporation of slightly more than half of the materials, while thermal evaporation from a boat was utilized in the balance of the cases.

Clean substrate surfaces are a prerequisite for successful coatings. The slightest amount of contamination can cause an immense amount of harm in the coating deposition process as well as an increase in surface absorption. Cleaning is an art rather than a science and, therefore, there is a great diversity of opinion on what constitutes a "good" procedure for cleaning substrates prior to coating them. A full treatment of various methods for cleaning glass substrates is given by Holland.[8] However, the sensitive nature of the highly polished surfaces of the fluoride windows requires the avoidance of such harsh cleaning procedures, since serious damage to the delicate optical surfaces can be the result of improper cleaning techniques.

The cleaning process utilized at Northrop to clean the fluoride windows prior to the deposition of the coating has been more or less conventional. Before the windows are placed into the system for coating, they are cleaned in a solution of detergent and warm water, then rinsed with distilled water and alcohol and blown dry with nitrogen gas. The coating system is pumped down to a pressure of less than 10^{-6} Torr and a pressure of less than 5×10^{-6} Torr is maintained during the coating deposition. The windows are heated to the desired substrate temperature and just prior to coating deposition they are subjected to a glow discharge cleaning. So far this procedure has been adequate for cleaning the fluoride surfaces prior to the deposition of antireflection coating designs, and for calorimetric absorption measurements.

TABLE 3. DEPOSITION PARAMETERS

MATERIAL	METHOD OF EVAPORATION	SUBSTRATE TEMPERATURE	DEPOSITION PRESSURE (TORR)	DEPOSITION RATE
Al_2O_3	E-Beam	200°C	5×10^{-5}	~600 Å/Min
LaF_3	Mo Boat	200°C	8×10^{-6}	~1800 Å/Min
MgF_2	E-Beam	200°C	2×10^{-6}	~1800 Å/Min
MgO	E-Beam	200°C	6×10^{-5}	~1200 Å/Min
PbF_2	E-Beam	200°C	7×10^{-6}	~1800 Å/Min
SiO	Ta Boat	200°C	$<1 \times 10^{-6}$	~3000 Å/Min
SrF_2	Mo Boat	200°C	8×10^{-6}	~1800 Å/Min
ThF_4	E-Beam	200°C	4×10^{-6}	~1800 Å/Min
ZnS	Ta Boat	150°C	8×10^{-6}	~1800 Å/Min
ZnSe	Ta Boat	150°C	4×10^{-6}	~1800 Å/Min

3. COATING STRUCTURE, ORIENTATION, AND GROWTH.

Crystal structures, preferred orientation, and growth characteristics of thin films investigated under this contract are detailed in this section. X-ray diffraction, utilizing a General Electric XRD-6 diffractometer with a copper-target tube operated at 35kV and 18 mA, provided the raw data. A nickel filter was used to obtain CuK_α radiation (λ = 1.5405 Å). Patterns were taken using a scan speed of 2° (2θ) per minute and a time constant of 0.5 in all cases, slit widths, detector sensitivity, and gain settings were varied as required to obtain optimum resolution and peak height. Tabulated values of d vs. 2θ obtained from the Bragg law, $n\lambda = 2d \sin\theta$, were used to reduce the data.

The thin film materials are grouped and discussed on the basis of chemical composition, i.e. fluorides, oxides, selenides and sulfides. Within each group, they are arranged in alphabetical order, i.e. LaF_3, MgF_2, PbF_2, ...

Lanthanum Fluoride, LaF_3 –

LaF_3 crystallizes in the hexagonal system with space group $P6_3/mmc$; the unit cell dimensions are given as a_o = 7.184Å, c_o = 7.351 on the ASTM card (#8-461), while Wyckoff[9] gives a_o = 3.148Å. Experimental results of x-ray diffraction scans of LaF_3 films (halfwave at 3.8 μm) on three different orientations of CaF_2 substrates are presented in tables 4, 5, and 6. Two salient features of these results are the moderate to strong preferred orientation in the films with some evidence of correlation with the substrate orientation and the strong peaks attributable to LaOF, La_2O_3, and LaO OH occurring on (100) and (111) substrate orientations.

TABLE 4. Results of X-Ray Diffraction Study of LaF_3 on CaF_2 Substrate.

Substrate Orientation: 1° Λ (100)

Film Thickness: 12,500 Å (λ/2 at 3.8 μm)

Radiation: CuK_α 35 kV. 18 mA. Ni Filter

Material	Card Ref.	Obs d (Å)	Obs I/I 100	ASTM d (Å)	ASTM I/I 100	hkl	Notes
LaF_3	8-461	3.587	03	3.59	32	110	
		3.223	08	3.229	100	111	
		2.070	03	2.075	51	300	
		1.8024	04	1.8064	33	302	
		1.0066	04	1.0078	03	117	
La OF	6-0281	1.5087	100	1.503	05	432	
LaO OH	19-656	3.015	02	3.04	60	$10\bar{2}$, 002	
CaF_2	4-0864	2.724	63	2.732	--	200	
		1.3633	>100	1.366	12	400	

TABLE 5. Results of X-Ray Diffraction Study of LaF_3 on CaF_2 Substrate.

Substrate Orientation: 3° Λ (110)

Film Thickness: 12,500 Å (λ/2 at 3.8 μm)

Radiation: CuK_α 35 kV. 18 mA. Ni Filter

Material	Card Ref.	Obs d (Å)	Obs I/I 100	ASTM d (Å)	ASTM I/I 100	hkl	Notes
LaF_3	8-461	3.587	02	3.59	32	110	
		2.067	100	2.075	51	300	
		1.8057	26	1.8064	33	302	
		1.3329	03	1.3354	15	411	
		1.1872	02	1.1877	14	413	
		1.0357	03	1.0370	03	600	
La_2O_3	22-641	2.293	04	2.298	04	$20\bar{4}, \bar{5}03$	

TABLE 6. Results of X-Ray Diffraction Study of LaF_3 on CaF_2 Substrate.

Substrate Orientation: 1° Λ (111)

Film Thickness: 12,500 Å (λ/2 at 3.8 μm)

Radiation: CuK_α 35 kV. 18 mA. Ni Filter

Material	Card Ref.	Obs d (Å)	Obs I/I 100	ASTM d (Å)	ASTM I/I 100	hkl	Notes
LaF_3	8-461	3.672	76	3.67	40	002	
		3.580	18	3.59	32	110	
		2.070	04	2.075	51	300	
		1.8364	10	1.8377	05	004	
		1.8024	03	1.8064	33	302	
		1.7400	06	1.7451	20	221	
		1.2239	03	1.2254	02	006	
		1.619	01	1.1601	02	116	
La_2O_3	5-0602	3.477	100	3.41	34	100	1
	24-554			3.51	30	100	
CaF_2	4-0864	3.1399	>100	3.153	94	111	
		1.5751	28	1.5765	--	222	

1. The spacing of 3.41 Å corresponds to a hexagonal form of La_2O_3 at room temperature, while 3.51 Å was obtained on the material at 2100° C. Hence, it appears that a high temperature form of the oxide is quenched in the thin film at room temperature.

If LaF_3 exhibits a preferred orientation on (100) CaF_2, it would appear to be (111). However, the other peaks of near half the (111) intensity indicate a high degree of randomness in the thin film orientation. On the other hand the single strong peak arising from LaOF indicates a very strong preferred orientation in that phase. The source of the latter material is undoubtedly the coating raw material itself, which contains an abundance of it (table 2).

On (110) CaF_2, LaF_3 shows a strong (100) preferred orientation as indicated by the intensity of the (300) peak in table 5. It appears that an appreciable fraction of crystallites in the coating material have taken a (302) orientation. The interplanar spacing of LaF_3 in these two orientations is within approximately 7% of the CaF_2 (220) spacing in the (110) direction (i. e. normal to the [110] substrate surface). This indicates influence of the coating orientation by the substrate structure.

The La_2O_3 peak on (110) CaF_2 is not particularly strong. Although substantially equal quantities of contaminants should deposit on all substrate orientations in films of this thickness, it is possible that the crystallite size of this material is very small and orientation near random, so that diffraction peaks are very weak.

On (111) CaF_2, LaF_3 exhibits a strong (001) preferred orientation, with a minority of crystallites oriented near (100) and (110). This orientation of (hexagonal) LaF_3 corresponds to the 3-fold symmetry of the (111) CaF_2 surface. The single La_2O_3 peak is again very strong, showing marked preferred orientation and an appreciable quantity of material. The large spacing may indicate that a high temperature form of the oxide is quenched in the thin film at room temperature.

On SrF_2, LaF_3 films show preferred orientation similar to that on CaF_2. On (100) SrF_2, LaF_3 has a predominantly (111) orientation with strong (100) and (110) type peaks, again indicating a high degree of randomness as on CaF_2 (100). On SrF_2 (110), LaF_3 shows a strong (110) orientation, unlike its behavior on (110) CaF_2. $La(OH)_3$ shows one strong peak (201), indicating strong preferred orientation of this impurity on (110). In addition, the patterns for both (110) and (111) SrF_2 substrates indicate significant microcrystalline or amorphous material with spacings in the 4 to 6Å region. The orientation of LaF_3 on (111) SrF_2 is again the basal (001) orientation shown on CaF_2. Relative growth rates of LaF_3 on CaF_2 and SrF_2 are indistinguishable for the three orientations studied, as reported in the previous quarterly report dated May, 1977 (figures 1 and 2 of that report).

Magnesium Fluoride, MgF_2 –

Magnesium Fluoride crystallizes in the tetragonal cassiterite (SnO_2) structure[10, 11] with space group P4/mnm, $a_o = 4.623$Å, $c_o = 3.052$ Å, Z = 2. Another form designated α - MgF_2, also tetragonal, with cell dimensions $a_o = 9.927$Å $c_o = 6.172$Å has been reported[12].

On CaF_2 (100), it takes a strong (001) orientation, with slightly smaller (002) spacing (1.511Å) than the tabulated value of 1.526Å. Very weak α- MgF_2 (440) and (216) lines are also observed with the tabulated spacings.

On CaF_2 (110), MgF_2 (211) and (112) have equal intensity, while (110) has 70% of this maximum intensity. Hence, this is a more or less randomly oriented film. On CaF_2 (111), a very weak α - MgF_2 (800) line is observed at 1.161Å. The only other diffraction line in the pattern not arising from the substrate has a spacing of 3.477Å, or three times the α- MgF_2 (800) spacing. This may indicate a distorted α - MgF_2 structure

with strong preferred orientation. On SrF_2, MgF_2 coatings are highly stressed and exhibit crazing and other defects. They show no X-ray diffraction peaks, indicating either that no long range order is developed or that crystallites are too small to diffract X-rays to yield significant peaks. Growth rates of MgF_2 on both CaF_2 and SrF_2 are indistinguishable among (100), (110), and (111) substrate surfaces.

Lead Fluoride PbF_2 -

PbF_2 crystallizes in two polymorphs with a transition temperature near 250°C. One of these, α - PbF_2, is orthorhombic with space group Pbnm, and lattice parameters $a_o = 7.357$Å, $b_o = 4269$Å, $c_o = 3.891$Å.[10] The unit cell contains four formula units of PbF_2. This structure is of the $PbCl_2$ type, in essence a distorted cubic close packing of halogen atoms with lead atoms accommodated in the same plane with them[10]; this phase has a higher atomic packing density than the cubic β - phase and hence should be stable at lower temperatures. The cubic β - PbF_2 polymorph has the fluorite structure with space group Fm3m and unit cell dimension $a_o = 5.927$Å; the unit cell contains four formula units of PbF_2.[10] It was found previously that both phases occurred in quarterwave thicknesses (at 5.3 μm) of PbF_2 deposited on single crystal CaF_2 substrates maintained at 200°C, with the cubic β - phase predominating and taking an orientation parallel to the substrate, with a mismatch of the order of 8%.[13] The growth rate of these films was found to vary with substrate orientation, being ~ 3% faster on (110) than on (100) and (111).

Results of the present work are presented in tables 7, 8, and 9. On CaF_2 (100), β - PbF_2 takes a very strong (111) preferred orientation, with minor (331) and (511) lines. This contrasts sharply with the previous X-ray and electron diffraction results, which showed a (100) orientation throughout the bulk of the film and a (110) orientation near the free surface.

TABLE 7. Results of X-Ray Diffraction Study of PbF_2 on CaF_2 Substrate.

Substrate Orientation: 1° Λ (100)

Film Thickness: 10,900 Å (λ /2 at 3.8 μm)

Radiation: CuK_α 35 kV. 18 mA. Ni Filter

Material	Card Ref.	Obs d (Å)	Obs I/I 100	ASTM d (Å)	ASTM I/I 100	hkl	Notes
β - PbF_2	6-0251	3.424	100	3.428	100	111	
		1.714	11	1.715	14	222	
		1.363	05	1.362	27	331	
		1.143	< 01	1.143	20	511	
α - PbF_2	6-0288	3.782	01	3.824	10	002	

TABLE 8. Results of X-Ray Diffraction Study of PbF_2 on CaF_2 Substrate.

Substrate Orientation: 5° Λ (110)

Film Thickness: 10,980 Å ($\lambda/2$ at 3.8 μm)

Radiation: CuK_α 35 kV. 18 mA. Ni Filter

Material	Card Ref.	Obs d (Å)	Obs I/I 100	ASTM d (Å)	ASTM I/I 100	hkl	Notes
β - PbF_2	6-0251	3.424	100	3.428	100	111	
		2.097	98	2.100	73	220	
		1.711	06	1.715	14	222	

TABLE 9. Results of X-Ray Diffraction Study of PbF_2 on CaF_2 Substrate.

Substrate Orientation: 1.8° Λ (111)

Film Thickness: 10,980 Å (λ/2 at 3.8 μm)

Radiation: CuK_α 35 kV. 18 mA. Ni Filter

Material	Card Ref.	Obs d (Å)	Obs I/I 100	ASTM d (Å)	ASTM I/I 100	hkl	Notes
β- PbF_2	6-0251	3.424	100	3.428	100	111	
		1.714	29	1.715	14	222	
		1.306	<01	1.328	21	420	
		1.142	02	1.143	20	511	
α - PbF_2	6-0288	3.798	05	3.824	10	002	
		1.2798	<01	1.2854	05	143	
		1.2470	<01	1.2570	03	224, 311	
CaF_2	4-0814	3.156	09	3.153	94	111	
		1.0515	<01	1.0512	07	511	

The α- PbF_2 in the present study is oriented near (001); in the previous work it showed a (012) orientation.

On the (110) surface of CaF_2, β - PbF_2 is the only phase present, showing equally strong (110) and (111) orientations (Table 8). In previous work, a very strong (110) orientation with minor (111) and α- PbF_2 (103) lines was determined.[13] On (111) CaF_2, the (111) orientation of β- PbF_2 predominates (Table 9), with minor (420) and (511) lines. The α - phase takes a predominant (001) orientation, with minor lines of higher index. The general behavior of PbF_2 on (111) CaF_2 is in accord with previous results.[13]

Present results on relative growth rates of PbF_2 on the three substrate orientations show fastest growth on (110) followed by (111) and (100), again in accord with previous results.[13] Hence, it is difficult to reconcile structure and growth rate data in the two sets of experiments. Present results suggest that the preferred growth direction of PbF_2 is [111] on all three substrate orientations. This is mitigated somewhat on (110) CaF_2, where the (110) line of β - PbF_2 has an intensity equal to (111). Reasons for this behavior are not clear. The degree of mismatch between the lattice parameters of coating and substrate materials, defined as

$$\Delta d = \frac{d_{hkl}\,(\text{coating}) - d_{hkl}\,(\text{substrate})}{d_{hkl}\,(\text{substrate})} \times 100\,\%$$

is about 8.7% for corresponding (100), (110), and (111) CaF_2 and βPbF_2. On (110) CaF_2, the mismatch with (111) PbF_2 is only 8.8%, so the coexistence of (111) and (110) PbF_2 on (110) CaF_2 is not surprising. However on (100) CaF_2, the mismatch with (111) PbF_2 is 37%.

The orientation of β - PbF_2 films on SrF_2 substrates follows substrate orientations nearly perfectly in all three cases as indicated by the data of tables 10, 11, and 12. This is not at all surprising, since the mismatch between corresponding planes of PbF_2 and SrF_2 is 2.4% for (100) and (110) and 2.3% for (111). α - PbF_2 occurs on the (100) substrate orientation with about equal (010) and (012) orientations; mismatch with the substrate is about 13% while that with β - PbF_2 is about 10%. No α - PbF_2 occurs on (110) SrF_2.

The presence of lead oxide, Pb_2O_3 on (110) and PbO on (111), comes as no surprise. It tends to increase the refractive index of the films slightly, but probably does not appreciably increase absorptance. The relative growth rates of PbF_2 on (110) and (100) SrF_2 are essentially equal, with the rate on (110) being slightly greater. The slowest growth rate is on (111) SrF_2.

Strontium Fluoride (SrF_2).

Strontium fluoride crystallizes in the cubic fluorite structure with space group Fm3m and lattice parameter a_o = 5.800Å; the unit cell contains four formula units of SrF_2.[10] It was found previously that SrF_2 films deposited on single crystal CaF_2 substrates took on very strong preferred orientations following the substrate.[13] However, its behavior is very similar to that of β - PbF_2 deposited on CaF_2 substrates. For halfwave thicknesses of SrF_2 on CaF_2 at design wavelengths of 3.8 and 5.3 μm, the dominant preferred orientation in the thin films is (111). For the 5.3 μm films, (100) and (110) type peaks are of very low intensity on the corresponding substrate orientations, with (111) always strongest. For the 3.8 μm films, the (100) and (110)-type peaks are about twice the intensity of the (111) peaks.

TABLE 10. Results of X-Ray Diffraction Study of PbF_2 on SrF_2 Substrate.

Substrate Orientation: 2.5° Λ (100)

Film Thickness: 5,490 Å (λ /4 at 3.8 μm)

Radiation: CuK_α 35 kV. 18 mA. Ni Filter

Material	Card Ref.	Obs d (Å)	Obs I/I 100	ASTM d (Å)	ASTM I/I 100	hkl	Notes
β - PbF_2	6-0251	2.957	100	2.970	56	200	
		1.4816	35	1.485	10	400	
α - PbF_2	6-0288	3.276	02	3.290	100	012	
		3.201	01	3.222	40	020	
		1.6407	01	1.6445	13	024	
		1.6040	04	1.6101	04	040	
SrF_2	6-0262	2.891	53	2.900	25	200	
		1.4485	71	1.4499	15	400	

TABLE 11. Results of X-Ray Diffraction Study of PbF_2 on SrF_2 Substrate.

Substrate Orientation: 2° Λ (110)

Film Thickness: 5490 Å (λ/4 at 3.8 μm)

Radiation: CuK_α 35 kV. 18 mA Ni Filter

Material	Card Ref.	Obs d (Å)	Obs I/I 100	ASTM d (Å)	ASTM I/I 100	hkl	Notes
β - PbF_2	6-0251	3.424	06	3.428	100	111	
		2.095	100	2.100	73	220	
		1.0485	05	1.050	08	440	
Pb_2O_3	23-331	2.319	02	2.317	02	003	

TABLE 12. Results of X-Ray Diffraction Study of PbF_2 on SrF_2 Substrate.

Substrate Orientation: 0.5° Λ (111)

Film Thickness: 5490 Å (λ/4 at 3.8 μm)

Radiation: CuK_α 35 kV. 18 mA. Ni Filter

Material	Card Ref.	Obs d (Å)	Obs I/I 100	ASTM d (Å)	ASTM I/I 100	hkl	Notes
β - PbF_2	6-0251	3.418	100	3.428	100	111	
		1.7098	07	1.715	14	222	
		1.1406	01	1.143	20	511	
α - PbF_2	6-0288	3.782	03	3.824	10	002	
		1.8937	< 01	1.912	16	004	
PbO	5-0561	2.506	< 01	2.510	18	002	

Diffraction lines corresponding to elemental strontium and its oxides are found on all substrate orientations, but in greater numbers and greater intensities on (100) and (111).

Thus it appears that the preferred growth direction of SrF_2 films is [111] on CaF_2 substrates, but the substrate orientation has a variable influence upon this, possibly corresponding to substrate temperature or impurity content of the films. Non-stoichiometry and the presence of oxygen or hydroxyl groups are problematic, as observed in previous work.[13] No difference in growth rate of SrF_2 among the three CaF_2 substrate orientations was found in the present work.

Thorium Fluoride (ThF_4)

Thorium tetrafluoride crystallizes in the monoclinic system with the zirconium fluoride structure.[9] Two unit cells of slightly different dimensions have been reported in recent entries in the ASTM card file.[14] These are $a_o = 13\text{Å}$, $b_o = 11.1\text{Å}$, $c_o = 8.6\text{Å}$, $\beta = 126.0°$ and $a_o = 12.9\text{Å}$, $b_o = 10.93\text{Å}$, $c_o = 8.58\text{Å}$, $\beta = 126.4°$, with space group C 2/c and cell content Z = 12 formula units of ThF_4. In the older literature,[9] a body-centered cell (I 2/c) was chosen, with dimensions $a_o = 10.64\text{Å}$, $b_o = 11.0\text{Å}$, $c_o = 8.6\text{Å}$, $\beta = 94°50'$, Z = 12.

On (100) CaF_2, ThF_4 films are crystalline with nearly equal (270) and ($21\bar{3}$) preferred orientations. Mismatch of ThF_4 (270) with the (100) spacing of CaF_2 is approximately 11%; mismatch of ($21\bar{3}$) with (200) CaF_2 is less than 1%. On (110) CaF_2, ThF_4 films are microcrystalline (amorphous to X-ray) with subequal diffuse maxima in diffracted X-ray intensity at approximately 3.8Å and 2.01Å, corresponding respectively to ThF_4 (220) and (103).[14] Mismatch between ThF_4 (220)

and CaF_2 (110) is 1.6% while that between ThF_4 (103) and CaF_2 (220) is 4.8%. On (111) CaF_2, ThF_4 is crystalline, taking a very strong $(32\bar{1})$ orientation, with one weak (332) line. Mismatch between CaF_2 (111) and ThF_4 $(32\bar{1})$ is approximately 9%; that between ThF_4 (332) and CaF_2 (222) is approximately 10%.

These results are in general accord with previous work, but details of the preferred orientations differ. This is not surprising since overall behavior remains the same: ThF_4 films tend to adopt a preferred crystallographic orientation leading to minimal mismatch with a CaF_2 substrate. Since the structure of ThF_4 is more complex than that of CaF_2, several interplanar spacings may lie near a given CaF_2 spacing. The particular orientation adopted by the film may then depend upon other considerations than mismatch across the film-substrate interface, e.g. contaminants, stacking faults, and preferential growth directions in the film material itself.

ThF_4 coating material from two different vendors (Cerac and Balzers) was deposited on SrF_2 substrates. Although the number and intensity of diffraction peaks attributable to oxides, oxyfluorides, and hydrated fluorides of thorium differ in thin films deposited using raw material from different vendors, the overall structure and orientation of the films is remarkably consistent.

On (100) SrF_2 the strongest coating diffraction line for Cerac material is attributable to hydrated ThF_4 with an observed spacing of 3.20Å corresponding to a strong (132) preferred orientation. The line of secondary intensity is attributable to ThF_4 (252) with a spacing of 1.61Å. Minor amounts of amorphous or microcrystalline material with spacings in the 5 to 9Å region, corresponding to ThF_4 (200) and (110) are observed.

For Balzers ThF_4, the coating is microcrystalline with primary orientation near (512) with an observed spacing of 1.466Å and subequal secondary orientations near (103) (d = 2.004Å) and (220) (d = 3.80Å). Mismatch between the (512) spacing and (400) SrF_2 is 1%, that between (103) and (220) SrF_2 (exposed on the SrF_2 (100) surface) is 2%, and that between (220) and (111) SrF_2 is 13%.

On (110) SrF_2, ThF_4 comprises predominantly well crystallized material with a strong ($52\bar{1}$) orientation (d = 2.27Å), a mismatch of 10.7% with (220) SrF_2 for films fabricated using material manufactured by either Cerac or Balzers. Both materials show minor amounts of poorly crystallized thin film with spacings corresponding to ThF_4 ($31\bar{1}$), (220), (030), ($31\bar{2}$), ($32\bar{1}$) and (310). Evidence for a substantial amount of microcrystalline, hydrated ThF_4 with a spacing of approximately 3.48Å was observed in a pattern from one coating fabricated from Cerac material.

On (111) SrF_2, ThF_4 from either vendor is crystalline, taking a strong (030) orientation, with an observed spacing of 3.697Å, a mismatch of 10.3% with the substrate (111) spacing of 3.35Å. Material with a spacing of 1.85Å, corresponding to (322) ThF_4 is also observed, giving rise to a diffracted X-ray intensity about 25% of the (030) line. Minor amounts of hydrated ThF_4 with a spacing of 2.45Å, corresponding to a (151) orientation are found in films fabricated from Cerac material, but not in those fabricated from Balzers material.

In summary of ThF_4 characteristics, it appears that the material may be crystalline, microcrystalline, or amorphous, depending upon substrate type and orientation. When crystalline, it tends to take an orientation which minimizes mismatch with the fluoride substrate spacing.

Hydrated material in thin film form is more common when Cerac raw material is used. Growth rates are indistinguishable among the three orientations of either substrate material.

Aluminum Oxide (Al_2O_3).

Although Al_2O_3 may crystallize in a multiplicity of forms, we shall be concerned only with the common form known variously as α - Al_2O_3, corundum, or sapphire. The structure is most easily visualized as a hexagonal close-packing of oxygen ions with small metallic ions lying in some interstices.[9] The space group is R $\bar{3}$ c and the structure may be referred to a primitive rhombohedral cell having a_o = 5.128Å, α = 55°20' and containing two formula units of Al_2O_3.[9] Alternatively, it may be referred to a hexagonal cell having a_o = 3.763Å, and containing six formula units of Al_2O_3.

On (100) CaF_2, Al_2O_3 films are crystalline with the corundum structure and a very strong (018) preferred orientation.[15] A small amount of material takes a (1 2 10) orientation and a minor amount of microcrystalline material having spacings in the 3 to 5 Å region is observed. On (110) CaF_2, the film is microcrystalline or amorphous with spacings in the 1.8 to 2.1Å region, corresponding to spacings for several different forms of aluminum oxide. On (111) CaF_2, Al_2O_3 films are largely microcrystalline or amorphous with spacings in the 5.9 and 7.4Å regions. A single, sharp peak at a spacing of 3.497Å corresponding to α -Al_2O_3 (012) is of low intensity, indicating that crystallinity is poorly developed on this substrate orientation.

On SrF_2, Al_2O_3 is apparently entirely amorphous to X-rays on two of the three substrate orientations, (100) and (110). On (111) SrF_2, microcrystalline material predominates with a spacing in the 6Å region. In

addition, a single weak peak at 3.69Å is observed. This is not attributable to common phases of Al_2O_3, $Al(OH)_3$, AlF_3, or elemental Al, or to the SrF_2 substrate. On both CaF_2 and SrF_2 the relative growth rate of Al_2O_3 is slowest on (111) and equally fast on (100) and (110).

Magnesium Oxide (MgO).

Magnesium oxide (periclase) crystallizes in the cubic sodium chloride structure with space group Fm3m and lattice parameter a_o = 4.211Å.[10] Recently reported experimental work with thin films of MgO on amorphous substrates[15] indicates that the preferred growth direction is < 111 >, independent of substrate temperature and deposition rate. Our results on oriented single crystal CaF_2 substrates tend to confirm this for the (100) and (110) substrate orientations, but not for the (111) orientation.

On (100) CaF_2, MgO films take a strong (111) orientation with a slightly expanded (111) spacing (2.496Å as compared to the expected 2.431Å).[16] A weak MgO (220) peak is also observed, with a 1.506Å (near nominal) spacing. On (110) CaF_2, the strongest MgO peaks again correspond to (111) and (222), with (111) having the expanded spacing observed on (100) CaF_2. The (222) spacing has the nominal value. Peaks corresponding to (100) and (110) MgO are also observed, with intensities 20 to 33% of the (111) intensity, indicating that appreciable fractions of crystallites in the MgO film are oriented in these directions. Mismatch of (111) MgO on (100) or (110) CaF_2 is about 9%, as is (100) MgO on (110) CaF_2 and (110) MgO on (100) CaF_2, so these observed combinations are not unexpected. However, the mismatch of (110) MgO on (110) CaF_2 is 23%, so this observed orientation is unexpected.

On (111) CaF_2, the only diffraction line not attributable to the substrate

corresponds to a spacing of 3.50Å, which is not identifiable with any known spacing of MgO, MgO_2, $Mg(OH)_2$ or elemental Mg. However, this spacing is close to double the $Mg(OH)_2$ (102) spacing of 1.794Å[17] or the MgO_2 spacing of 1.700Å.[18] Thus, the formation of a magnesium oxide or hydroxide superstructure in the thin film form is a possibility on the (111) CaF_2 surface.

On SrF_2, MgO films are apparently largely amorphous to X-ray and exhibit stoichiometry problems. On (100) SrF_2, a weak MgO (111) diffraction peak occurs with the nominal 2.43Å spacing, in addition to a strong peak with a spacing of 3.22Å. This is almost exactly double the (110) spacing of elemental Mg[19] and could imply formation of a Mg superstructure. The Mg (200) line also occurs on this substrate orientation. On (110) SrF_2, the material is microcrystalline with spacings in the 4.5Å and 3.8Å regions. One weak diffraction peak at 2.266Å is attributable to α- MgF_2[12] (222, 410). On (111) SrF_2, the material is again microcrystalline with spacings in the 5.9Å region.

On CaF_2, MgO films show no variation in refractive index with substrate orientation, but different growth rates are observed. The growth rate on (100) CaF_2 is fastest, corresponding to the strongest (111) preferred orientation in the MgO film. On (110) and (111) CaF_2, growth rates are about equal and slower than on (100), corresponding to the poorer preferred orientation and formation of superstructures. On SrF_2, both growth rates and refractive indices vary with substrate orientation, greatest index and fastest growth rate occurring on (110), slowest growth and lowest index on (100), intermediate rates and index on (111). Material on (100) CaF_2 is generally crystalline while that on (110) and (111) is amorphous or microcrystalline.

Silicon Monoxide, SiO.

SiO films are non-stoichiometric, but mechanically and chemically very stable and can be used as excellent coatings for the infrared region.[7] They are nominally amorphous to X-ray and electron diffraction, but weak diffraction peaks corresponding to SiO_2 or elemental silicon are not unexpected.

On (100) CaF_2, SiO deposits with one strong tridymite (unindexed) peak with a spacing of 1.507Å.[20] No microcrystalline material is evident on this substrate orientation. On (110) CaF_2, it deposits as amorphous or microcrystalline material with spacings of the order of 1.9Å, also indicative of the tridymite phase of SiO_2[20] and of elemental silicon.[21]

On (111) CaF_2, SiO deposited as amorphous or microcrystalline material with spacings in the 1Å and 6.3Å regions in two of three cases studied. In the third case, a very strong tridymite[20] peak was observed at 3.49Å, indicating a strongly oriented, well crystallized deposit. Minor amounts of microcrystalline material with a spacing of approximately 5.9Å were also observed in this film. Growth rates of SiO are fastest on (100) CaF_2, slowest on (110), and intermediate on (111).

On SrF_2 (100), SiO films are amorphous or microcrystalline with spacings in the 1.41 and 1.46Å regions, corresponding to the tridymite phase of SiO_2.[20] On (110) SrF_2, SiO films comprise both microcrystalline and well crystallized material. Microcrystalline material has spacings in the 4Å and 2.28Å regions, corresponding to tridymite. On (111) SrF_2, SiO films show microcrystalline material in the 4 - 9Å region and the 3.7Å region, corresponding again to tridymite. Growth rates of SiO on SrF_2 are fastest on (100), intermediate on (111) and slowest on (110).

Zinc Selenide (ZnSe).

Zinc selenide crystallizes in the cubic β - ZnS structure, with space group $F\bar{4}3m$ and lattice parameter 5.668Å.[10, 22] A hexagonal form with a_o = 3.996Å and c_o = 6.53Å has also been reported, although the space group is not given, the structure is most likely similar to the α - ZnS structure.

On both (100) and (110) CaF_2, cubic ZnSe films are deposited with a strong (111) preferred orientation,[23] as indicated in tables 13 and 14. Mismatch of (111) ZnSe with (100) and (110) CaF_2 is 20% and 15%, respectively.[22] On (111) CaF_2, ZnSe is deposited in the hexagonal form with very strong (100) preferred orientation,[23] as shown in table 15. On the latter substrate, several very weak peaks attributable to $ZnSeO_4$ are also evident, as indicated in table 15. Tables 13-15 provide a fair representation of the ZnSe structure on three sets of CaF_2 substrates. Growth rates of ZnSe on CaF_2 are fastest (and essentially equal) on (100) and (110) and slowest on (111).

This growth behavior correlates very well with the structural and orientational similarities of the films on (100) and (110) and the dissimilarity on (111).

On SrF_2 substrates, the tendency toward crystallization of ZnSe in the cubic form with the (111) preferred orientation is again seen on the (100) and (110) substrate orientations. However, peaks attributable to zinc oxides, hydroxides, and selenates are also present along with broad humps in the diffractometer traces arising from microcrystalline material with spacings in the 3 to 4Å region on (110). On the (111) orientation of the SrF_2 substrates, hexagonal ZnSe is again evident, but with a weak (103) or (105) orientation (rather than (100)). In addition, large amounts

TABLE 13. Results of X-Ray Diffraction Study of $ZnSe$ on CaF_2 Substrate.

Substrate Orientation: 0° Λ (100)

Film Thickness: 10,950 Å (λ/2 at 5.3 μm)

Radiation: Cu K_α 35 kV. 18 mA. Ni Filter

Material	Card Ref.	Obs d (Å)	Obs I/I 100	ASTM d (Å)	ASTM I/I 100	hkl	Notes
$ZnSe$	5-0522	3.270	100	3.273	100	111	
		1.0893	<01	1.0901	08	511	
$ZnSeO_4$	19-1476	3.608	03	3.645	100	111	
CaF_2	4-0864	1.3625	08	1.366	12	400	

TABLE 14. Results of X-Ray Diffraction Study of $ZnSe$ on CaF_2 Substrate.

Substrate Orientation: 8° Λ (110)

Film Thickness: 10,950 Å (λ/2 at 5.3 μm)

Radiation: Cu K_α 35 kV. 18 mA. Ni Filter

Material	Card Ref.	Obs d (Å)	Obs I/I 100	ASTM d (Å)	ASTM I/I 100	hkl	Notes
$ZnSe$	5-0522	3.270	100	3.273	100	111	
		1.0893	< 01	1.0901	08	511	
$ZnSeO_4$	19-1476	3.616	03	3.645	100	111	

TABLE 15. Results of X-Ray Diffraction Study of $ZnSe$ on CaF_2 Substrate.

Substrate Orientation: 1° Λ (111)

Film Thickness: 10,950 Å (λ/2 at 5.3 μm)

Radiation: CuK_α 35 kV. 18 mA. Ni Filter

Material	Card Ref.	Obs d (Å)	Obs I/I 100	ASTM d (Å)	ASTM I/I 100	hkl	Notes
ZnSe	15-105	6.50	05	----	---	001 ?	1
		3.490	100	3.43	100	100	
ZnSeO4	20-1449	4.84	03	4.94	85	011, 111	
ZnSeO4	19-1476	3.767	02	3.76	35	021	
		3.616	02	3.645	100	111	
		1.745	06	1.756	02	142	
		1.576	05	1.582	02	114	
		1.163	10	1.168	02	172, 314	
CaF_2	4-0864	3.151	>100	3.153	94	111	
		1.0515	21	1.0512	07	511	

1. d(002) = 3.25 Å; d(001) Not Listed.

of microcrystalline material with spacings in the 5-7Å region are evident on the (111) substrate orientation.

Growth rates of ZnSe on SrF_2 are fastest and about equal on (110) and (111) and slowest on (100). This behavior does not correlate well with the structural data, except for the presence of microcrystalline material on (110) and (111) and its absence on (100). This may mean that more rapid growth is associated with the formation of films having a lower degree of long range order.

Reasons for the differences in the coatings on SrF_2 and CaF_2 substrates are difficult to ascertain. Apparently, the crystal structure of the coatings on either substrate is not governed by the substrate structure or orientation for the deposition conditions employed to date. The predominant impurities on SrF_2 appear to be $Zn(OH)_2$, while those on CaF_2 appear to be $ZnSeO_4$, which may indicate the presence of small amounts of oxygen during deposition in the latter case. The hydroxide would imply the presence of water vapor in the deposition environment. These differences are not dependent on conditions in a single coating run, but represent results of at least three coating runs on each substrate material, or a total of nine samples.

Zinc Sulfide (ZnS).

Zinc sulfide crystallizes in two structures, the hexagonal α- ZnS or Wurtzite type having space group $P6_3mc$, and the cubic β - ZnS or Sphalerite type having space group $F\bar{4}3m$.[10] Both structures are based on tetrahedral coordination. In the cubic phase, zinc atoms are arranged on a face-centered cubic lattice while in the hexagonal form they fall into a distorted hexagonal close-packing. Lattice parameters

of the hexagonal phase are a_o = 3.820 Å, c = 250 Å while the cubic phase has a unit cell dimension a_o = 5.406 Å.

Alternative stacking arrangements in the c-axis direction of the hexagonal phase give rise to several polytypes of ZnS; the best known of these are designated 8H and 10H, with c-axis dimensions of 24.96 Å and 31.20 Å, respectively.[25]

On CaF_2 substrates, ZnS deposits in the hexagonal (Wurzite or α- ZnS) form, yielding diffraction patterns indicative of the 8H polytype.[25] On (100) and (110) substrate orientations the film orientation is predominantly basal with spacings of approximately 3.10 Å, or slightly smaller than the nominal 3.12 Å spacing between successive layers of Zn or S atoms.[26] The strongest diffraction peak on (100) CaF_2 corresponds to a spacing of 1.51 Å, less than half of the 3.12 Å fundamental ZnS spacing. This diffraction line is attributable to a form of α-$Zn(OH)_2$[27] with a spacing of 1.511 Å. However, the absorption results to be presented in the next section do not justify large amounts of the hydroxide material. It is thus possible that the 1.51 Å spacing corresponds to a basal ZnS spacing, considerably smaller than the nominal 1.56 Å.[24, 25] Minor diffraction lines on the (100) substrate orientation correspond to (110) ZnS(8H), at 1.905 Å, (300) ZnS (8H) at 1.102 Å, and α-$Zn(OH)_2$ (031) at 3.02 Å.

On (110) CaF_2 substrates, the situation is somewhat simpler, the strongest peak arising from the (008) spacing of ZnS (8H) at 3.11 Å. Lower intensity lines arise from (10 10), (10 13), and (110) spacings of the same material at 1.979, 1.943, and 1.887 Å (observed) and Wurtzite (102) at 2.24 Å.[024] No lines attributable to zinc oxides or hydroxides were observed.

On (111) CaF_2, ZnS again deposits in the hexagonal form with a strong preferred orientation. The strongest diffraction line corresponds to a spacing of 3.477 Å, which is very nearly three times the α - ZnS (212) spacing of 1.161 Å, also observed on these substrates. The 3.477 Å spacing does not correspond to diffraction lines for common oxides, hydroxides, sulfites, sulfates, or fluorides of zinc or to elemental zinc or sulfur. In fact, the only (non-substrate) diffraction lines observed with this substrate orientation are at 3.477 Å, 1.161 Å, and 1.06 Å, the latter attributable to α - ZnS (213). Hence we conclude that the material takes a strong preferred orientation parallel to (212), but possibly has developed a superstructure having triple the (212) spacing.

Structural mismatch criteria between the substrate and film do not appear to govern the choice of structure and orientation in these ZnS films. These criteria would predict a cubic (sphalerite or β - ZnS) structure for films on CaF_2, with a strong preferred orientation paralleling the substrate, since the structures and spacings are similar to within 1%.[24, 28] On SrF_2, these same criteria would predict α - ZnS on all three substrate orientations, with (101) ZnS paralleling (100) SrF_2, (102) ZnS on (110) SrF_2 and (100) ZnS on (111) SrF_2.[24, 29] Some of these relationships are in fact observed.

On CaF_2, the growth rate of ZnS is fastest on (110), intermediate on (100) and slowest on (111), exhibiting no obvious correlation with the structural data, except that the structure is simplest and preferred orientation strongest on (110). No extraneous lines attributable to impurities are observed on (110), but they are observed on the other substrate orientations.

Results of X-ray diffraction investigations of ZnS films on SrF_2 substrates are detailed in Tables 16, 17, and 18. On (100) SrF_2 (Table 16) the predicted very strong (101) orientation of the α - ZnS film is observed. Mismatch between film and substrate spacings in this orientation is 9.9%. On (110) SrF_2 (Table 17), the predicted (102) orientation of α- ZnS is observed. Mismatch in this orientation is 11%. Minor lines corresponding to poorly crystalline material of the 10H polytype of ZnS are also observed on this substrate orientation; none of these correspond closely to the substrate spacing.

On (111) SrF_2, the predicted (100) α - ZnS film structure and orientation are not observed (Table 18). The observed orientation of the ZnS (10H) polytype corresponds to a mismatch of approximately 10% with the substrate.[25, 29] The predicted (100) orientation of α - ZnS on (111) SrF_2 would result in a mismatch of 1.3%.[24, 29]

The growth rate of ZnS is fastest on (110) SrF_2, slowest on (100), and intermediate on (111), correlating poorly with observed structure and orientation. Slow growth of the strongly oriented, well crystallized material with low mismatch on (100) SrF_2 is quite plausible, but the rapid growth in the (102) orientation on (110) SrF_2 is difficult to reconcile with the slower growth of the 10H polytype on (111), where both have a 10% mismatch with the substrate spacing and somewhat disordered structure.

4. COATING PROPERTIES

The coating properties of interest in this study are refractive index and absorption coefficient on the various substrate materials and orientations. In order to determine these properties, single layer films of quarterwave and halfwave optical thickness at appropriate wavelengths

TABLE 16. Results of X-Ray Diffraction Study of ZnS on SrF_2 Substrate.

Substrate Orientation: 3° Λ(100)

Film Thickness: 5995 Å (λ/4 at 5.3 μm)

Radiation: CuK_α 35 kV. 18 mA. Ni Filter

Material	Card Ref.	Obs d (Å)	Obs I/I 100	ASTM d (Å)	ASTM I/I 100	hkl	Notes
α - ZnS	5-0492	2.919	38	2.925	84	101	
		1.466	100	1.462	05	202	
SrF_2	6-0262	1.4515	80	1.4499	15	400	

TABLE 17. Results of X-Ray Diffraction Study of ZnS on SrF_2 Substrate.

Substrate Orientation: 0.8° Λ (110)

Film Thickness: 5995 Å (λ/4 at 5.3 μm)

Radiation: Cu K_α 35 kV. 18 mA. Ni Filter

Material	Card Ref.	Obs d (Å)	Obs I/I 100	ASTM d (Å)	ASTM I/I 100	hkl	Notes
α - ZnS	5-0492	2.271	100	2.273	29	102	
		1.1337	16	1.1364	<01	204	
Zn S(10H)	12-688	3.113	06	3.12	100	0 0 10	
		2.81	02	2.81	02	106	1
		2.469	01	2.49	02	--	2
SrF_2	6-0262	2.052	>100	2.0508	80	220	
		1.0253	>100	1.0253	07	440	

1. Very broad and poorly defined; microcrystalline or amorphous material.

2. The (002) spacing of elemental zinc is 2.473Å, and is thus indistinguishable from this one, within experimental error.

TABLE 18. Results of X-Ray Diffraction Study of ZnS on SrF_2 Substrate.

Substrate Orientation: 0° Λ (111)

Film Thickness: 5995 Å (λ/4 at 5.3 μm)

Radiation: Cu K_α 35 kV. 18 mA. Ni Filter

Material	Card Ref.	Obs d (Å)	Obs I/I 100	ASTM d (Å)	ASTM I/I 100	hkl	Notes
ZnS(10H)	12-688	3.6972	100	----	---	---	1
		1.8486	16	1.841	02	1 0 14	
		1.2339	13	1.239	04	ni	2
ZnS_2O_4	1-0162	~5.9	~50	5.88	100	ni	3
SrF_2	2-0262	3.336	>100	3.352	100	111	
		1.6710	86	1.6743	05	222	
		1.1149	60	1.1164	16	511	

1. Not Listed; this spacing is exactly 2 times the observed (1 0 14) spacing of ZnS(10H).

2. Other materials having similar spacings include elemental zinc (004), 1.237 Å and ZnO (202), 1.238 Å.

3. Broad, poorly defined; Microcrystalline or Amorphous phase with spacing corresponding to this material.

(3.8 μm and/or 5.3 μm) were deposited on one surface of CaF_2 and/or SrF_2 substrates having nominal (100), (110), and (111) orientations.

Refractive indices were obtained from infrared transmission measurements of the quarterwave films, while absorption coefficients were measured on the halfwave films. Information on relative growth rates was obtained from spectrophotometer transmission scans of the halfwave coated samples in the visible region (600 to 800 nm), as reported in the previous section. Refractive index and absorption results are reported here, with footnotes on relative growth rates of the films added for purposes of correlation.

In order to obtain absorptance values (β and k) for halfwave thicknesses of coating materials, absorptances for the uncoated substrates must be known. The determination of the absorption coefficient of a coating material on a substrate which is transparent in the wavelength region of the irradiating laser is in principle quite straightforward. The total absorption due to a coating of specified thickness is obtained as a difference in total absorption between coated and uncoated substrates. Sequential measurements on the same substrate are utilized to obtain either a difference in absorption between coated areas or a difference in absorption in a single location before and after coating. The former method has the advantages of speed and ease of verification, but substrate inhomogeneity can cause difficulties. In the latter method, substrate inhomogeneity is eliminated, but verification of the absorption measurement on the uncoated substrate is problematic.

For an uncoated transparent substrate irradiated by a laser beam in a standard adiabatic calorimeter configuration, the total absorption A_o is given by[30]

$$A_o = \frac{2n_s}{1 + n_s^2} \qquad P_A / P_T \tag{1}$$

where n_s is refractive index of the sample, P_A is power absorbed by the sample, and P_T is the power transmitted through the sample. If the masses and heat capacities of the sample and calorimeter cone are known and irradiation times are held constant for a given series of measurements, the absorption is proportional to the ratio of output voltages from the sample and power cone thermocouples.

The total absorptance calculated from (1) includes both surface and bulk contributions. The absorption coefficient for this substrate is

$$\beta = A_o / \ell \tag{2}$$

where ℓ is the sample thickness; again, both surface and bulk contributions are included. If a coating is subsequently deposited upon such a substrate and a new absorption measurement made, the total absorptance takes on a value

$$A_t = A_o + A_1 \tag{3}$$

where A_1 is the increase in total absorptance due to the coating alone. For the case of a coating of halfwave optical thickness, A_1 can be evaluated using (1) and (3) since the surface reflectivity of the coated sample is identical to that of the uncoated substrate and the parenthetical factor involving n_s in (1) remains unchanged.

To obtain an absorption coefficient for a coating of physical thickness t_1 from a measured value of A_1, we employ a formula of Loomis,[31] with minor rearrangement,

$$\beta_1 = \frac{A_1 n_1}{2t_1 n_o} \quad \frac{(n_o + n_s)^2 \cos^2 \varphi_1 + [n_1 + (n_o n_s / n_1)]^2 \sin^2 \varphi_1}{n_1^2 + n_s^2}, \qquad (4)$$

where

n_1 = film refractive index

n_s = substrate refractive index

n_o = incident medium refractive index

$\varphi_1 = 2\, n_1 t_1 / \lambda_o$

λ_o = laser wavelength (vacuum).

For a single coating of thickness $\lambda_o / 2$, (4) reduces to

$$\beta_1 = \frac{A_1 n_1}{2t_1 n_o} \quad \frac{(n_o + n_s)^2}{n_1^2 + n_s^2} \qquad (5)$$

The absorption index of the thin film is then

$$k_1 = \frac{\lambda_o \beta_1}{4\pi} \qquad (6)$$

Hence, in order to obtain the absorption coefficient and absorption index of a single layer coating on a transparent substrate, we require only the refractive index of film and substrate, the physical thickness of the film, and two absorption measurements. The method of measuring the absorption has been discussed in the literature.[32, 33]

The spectral composition of the irradiating laser has been shown to be a significant variable in absorptance measurements at CO laser

wavelengths.[14, 16] In order to verify the spectral output of both the CO and DF lasers employed in the present measurements, spectra were analyzed using a Jarrell-Ash Model 78-466 scanning spectrometer with a 50 groove/mm grating blazed at 10.0 μm and a Ge:Au detector. Spectra for the CO laser have been reported previously.[32, 34] with centroids varying from 5.25 μm to 5.45 μm, depending upon CO partial pressure. In the present study, with operating parameters typical of those employed in the calorimetric measurements (i.e. 6 mm intracavity iris, total output power ~ 2.8 W), the mean centroid of two spectra run with identical parameters was 5.29 ± .04 μm, with a bandwidth of 0.57 ± 0.1 μm.

A typical output spectrum for the CO laser is illustrated in Figure 1. Table 19 is an attempt at quantitative characterization of the spectrum. In this table, the first column gives the wavelength of individual lines as measured with the spectrometer (in air). "Line Identification" (column 2) is obtained by comparison with published data. In the third column, the mean intensity of each line is divided by that of the strongest line (7-6, P(16)), to obtain a relative intensity scale for plotting in Figure 1. The fourth column gives the mean intensity of each line divided by the summed intensity of all measured lines. The tabulated number is the fraction of laser power in any line. The fifth column, headed $|\Delta \bar{I}|$ is the standard deviation of the relative intensities from which column 3 was prepared. This is divided by the sum of intensities and tabulated in the sixth column to indicate the variability of a given line as a fraction of the laser output.

The DF laser spectrum was also analyzed in some detail since the actual output of the laser in use in the calorimetry laboratory had not been characterized previously. The same spectrometer, grating, and detector

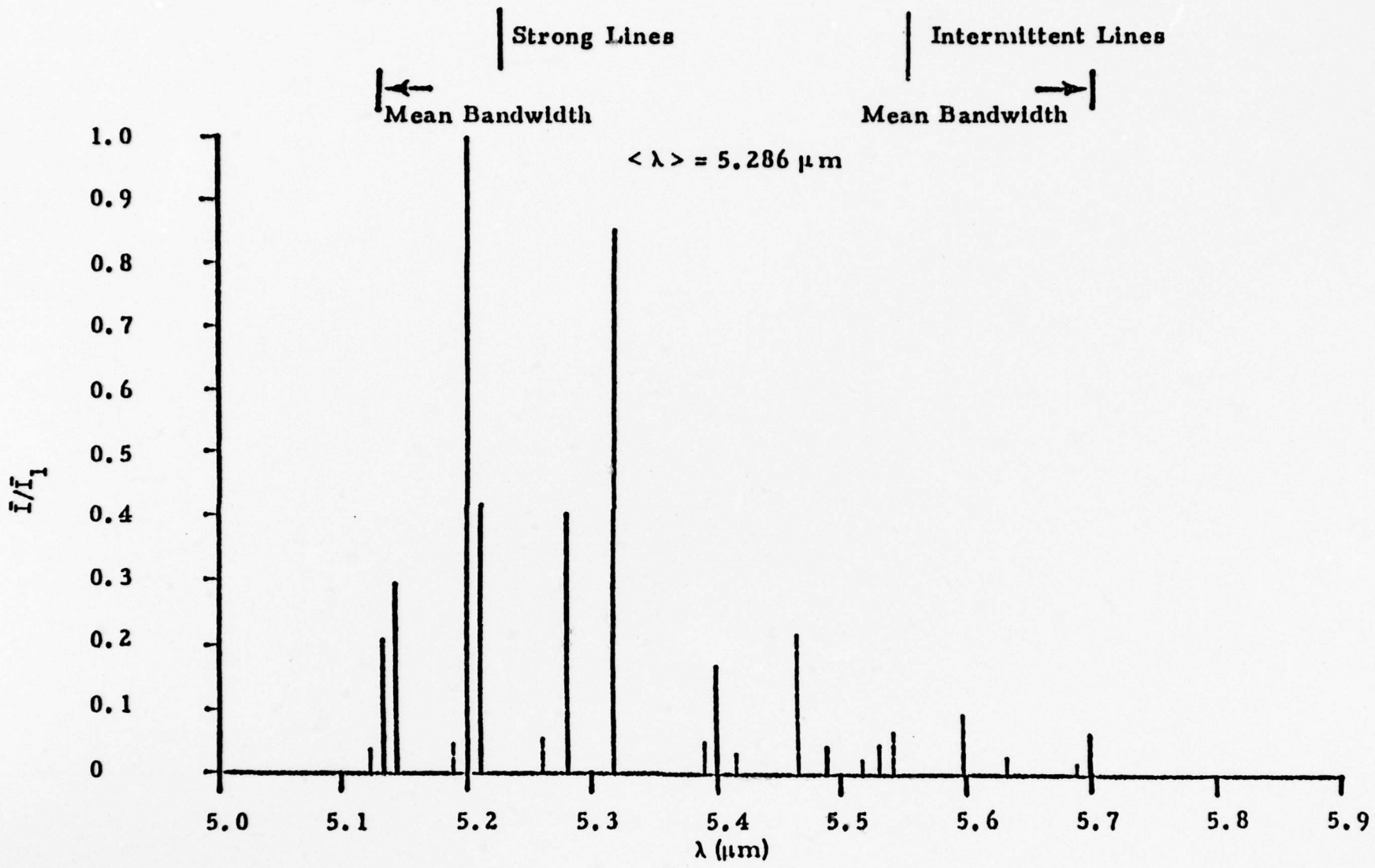


Fig. 1. Mean CO Laser Spectrum For 2 Runs With Identical Operating Parameters.

TABLE 19. Mean CO Laser Spectrum for 2 Runs with identical Operating Parameters. Mean centroid $< \lambda >$ is at 5.286 ± 0.04 μm. Mean Bandwidth is 0.57 μm. Output power is ~ 3 w, with a 6 mm diameter intracavity iris.

$\bar{\lambda}$ (μm)	Line Ident.	$\bar{I}/\bar{I}_1$	$\bar{I}/\Sigma\bar{I}$	$\lvert\Delta\bar{I}\rvert$	$\lvert\Delta\bar{I}\rvert/\Sigma\bar{I}$
5.1220	6-5, P(15)	0.037	0.009	0.052	0.012
5.1329	6-5, P(16)	0.211	0.051	0.030	0.007
5.1431	6-5, P(17)	0.292	0.070	0.071	0.017
5.1895	7-6, P(15)	0.038	0.009	0.054	0.013
5.1999	7-6, P(16)	1.000	0.240	0.000	0
5.2110	7-6, P(17)	0.420	0.101	0.303	0.073
5.2580	8-7, P(15)	0.054	0.013	0.076	0.018
5.2806	8-7, P(17)	0.412	0.099	0.112	0.027
5.3183	9-8, P(14)	0.854	0.205	0.130	0.031
5.3907	10-9, P(14)	0.050	0.012	0.071	0.017
5.40125	10-9, P(15)	0.169	0.041	0.115	0.028
5.4130	10-9, P(16)	0.031	0.007	0.044	0.011
5.4644	11-10, P(14)	0.223	0.054	0.315	0.076
5.4888	11-10, P(16)	0.043	0 010	0.061	0.015
5.5173	12-11, P(12)	0.020	0.005	0.028	0.007
5.5287	12-11, P(13)	0.044	0.011	0.063	0.015
5.5408	12-11, P(14)	0.062	0.015	0.088	0.021
5.5948	13-12, P(12)	0.090	0.022	0.127	0.030
5.6304	13-12, P(15)	0.022	0.005	0.031	0.007
5.6868	14-13, P(13)	0.012	0.003	0.0017	0.004
5.6976	14-13, P(14)	0.064	0.015	0.023	0.006
5.8394	16-15, P(12)	0.014	0.003	0.020	0.005

employed with the CO laser were used to analyze the DF. Typical operating parameters for calorimetric measurements were used. These include a helium partial pressure of ~4 Torr, with about 1.2 Torr each of SF_6 and D_2, and ~0.1 Torr of O_2 for a total of 6-8 Torr. The discharge tube is operated at a voltage of ~13 kV and current of ~450 mA to produce 2-4 W total power. Cavity temperature is ~65°C. Seven spectra were run over a three-day period and the results averaged to obtain a composite spectrum, presented in Figure 2 and Table 20.

In general, it appears that the overall spectrum is very stable with respect to centroid (~3.9 μm) and bandwidth (~0.3 μm), but individual lines are highly variable. Table 20 is an attempt at quantitative characterization of this aspect of the spectrum. In this table, the first column gives the wavelength of individual lines as measured with the spectrometer (in air). "Line Identification" (column 2) is obtained by comparison with published data.[17, 18] Column 3 ($\bar{I}$) gives the mean relative intensity of each line. The tabulated number was obtained by first determining the intensity of the line in question in each of the seven spectra, relative to the strongest line in that spectrum taken as 1.0, and then averaging the results over all seven spectra. (If a line was absent from a particular spectrum, its intensity was counted as 0.)

The mean relative intensities in column 3 of the table were divided by the sum of all of the mean intensities to obtain the fraction of the total laser energy in any given line, listed in the fourth column. The fifth column, headed "ΔI" gives the standard deviation of the mean relative intensities in column 3. This is divided by the sum of the intensities to determine the variability of a given line as a fraction of the total laser output and tabulated in the sixth column. In the seventh column, the mean relative intensity of each line is divided by that of the strongest line (2-1, P(10)), to obtain a relative intensity scale for plotting

Fig. 2 DF LASER SPECTRUM COMPILED FROM 7 RUNS OVER A 3-DAY PERIOD, OUTPUT POWER: 2-4 WATTS.

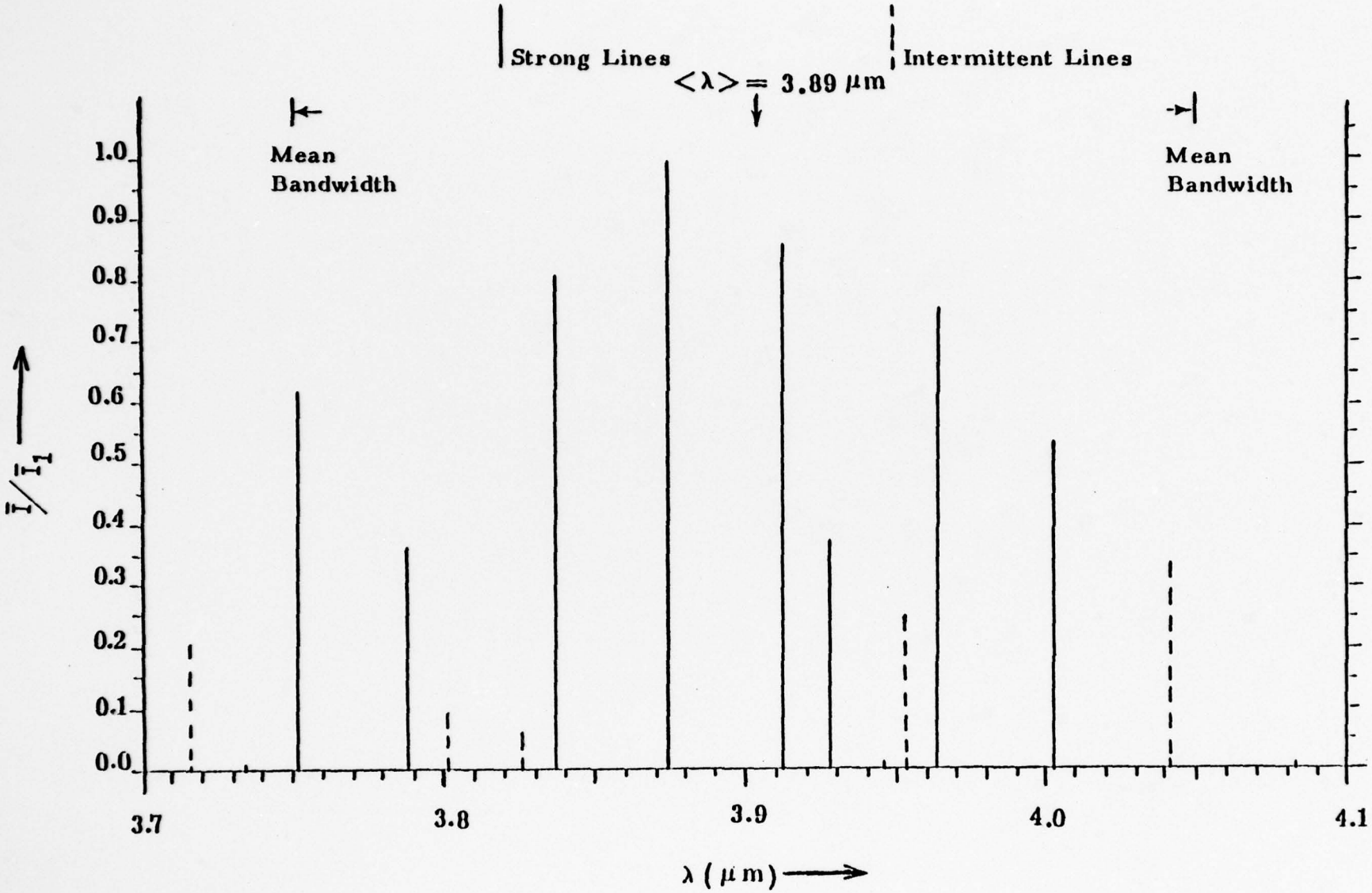


TABLE 20. DF Laser Spectrum Compiled from 7 Runs on 3 Days. Mean Centroid $\langle \lambda \rangle$ of All Spectra is 3.89 ± .025 μm. Mean Bandwidth of All Spectra is 0.297 μm ± 0.028 μm. For Individual Lines, Tabulated $\bar{\lambda}$ May Vary by ± 0.0007 μm From Run to Run.

$\bar{\lambda}$ (μm)	Line Ident.	$\bar{I}$	$\bar{I}/\Sigma\bar{I}$	$\lvert\Delta\bar{I}\rvert$	$\lvert\Delta\bar{I}\rvert/\Sigma\bar{I}$	$\bar{I}/\bar{I}_1$	No Runs Present
3.1760	1-0, P(9)	0.14	0.032	0.16	0.036	0.21	4
3.7514	1-0, P(10)	0.42	0.096	0.31	0.071	0.62	7
3.7880	1-0, P(11)	0.25	0.057	0.22	0.050	0.37	6
3.8262	1-0, P(12)	0.04	0.009	0.06	0.014	0.06	2
3.7337	2-1, P(6)	<0.01	<0.002	0.02	0.005	<0.01	1
3.8015	2-1, P(8)	0.07	0.016	0.12	0.027	0.10	2
3.8372	2-1, P(9)	0.55	0.125	0.42	0.096	0.81	7
3.8737	2-1, P(10)	0.68	0.155	0.27	0.062	1.00	7
3.9123	2-1, P(11)	0.59	0.134	0.38	0.087	0.86	7
3.9526	2-1, P(12)	0.18	0.041	0.19	0.043	0.26	4
3.9270	3-2, P(8)	0.26	0.059	0.25	0.057	0.38	5
3.9639	3-2, P(9)	0.52	0.118	0.33	0.075	0.76	7
4.0021	3-2, P(10)	0.36	0.082	0.28	0.064	0.53	6
4.0414	3-2, P(11)	0.30	0.068	0.40	0.091	0.44	4
4.0832	3-2, P(12)	<0.01	<0.002	0.02	0.005	<0.01	1
3.9457	4-3, P(5)	0.01	0.002	0.03	0.007	0.01	1

in Figure 2. Note that this number is also the fraction of total laser energy appearing in an individual line, relative to the strongest line in the composite spectrum. Finally, the last column of the table designates the number of spectra, (out of a total of 7) in which an individual line had non-zero intensity.

Results of the coating absorptance measurements carried out to date under the contract are presented in Tables 21-24, along with refractive indices determined from quarterwave films. The absorption coefficient, β, is tabulated rather than the absorption index, k, for convenience. The absorption index can of course be obtained from the β values using equation (6).

All values tabulated here differ from those presented in the previous quarterly report (May, 1977) as a result of recalculation using the program of Loomis[35] for a single layer film on the exit surface of a transparent window and correction of an error in the original calculation using equation (5).

Some general features of the data are worth noting. It appears that the coating materials fall into three broad groups, based on absorption; (1) those having β values between ~ 1 and ~ 7 cm^{-1}, (the low absorption group); (2) those having β values between ~ 9 and ~ 20 cm^{-1} (the intermediate group); and (3) those having β values of 20 cm^{-1} or more, ranging up to 100 cm^{-1} (high absorption group).

The sum of the standard deviation of the absorption measurements on the uncoated and coated substrate is a measure of the precision of the coating absorption determination. Since this determination involves the subtraction of two numbers with similar errors, the precision of

TABLE 21. ABSORPTION COEFFICIENTS OF FLUORIDE COATING MATERIALS MEASURED BY DF LASER CALORIMETRY ON COATINGS OF HALFWAVE OPTICAL THICKNESS AT A DESIGN WAVELENGTH OF 3.8 μm

COATING MATERIAL	REFRACTIVE INDEX	COATING ABSORPTION COEFFICIENT, β (cm^{-1}) CaF_2 SUBSTRATE (100)	(110)	(111)	SrF_2 SUBSTRATE (100)	(110)	(111)
LaF_3	1.52	41.49	28.43	24.88	36.61	24.53	29.49
MgF_2	1.36	19.06	21.70	21.17	17.56	18.33	19.20
PbF_2	1.73	4.24	3.03	7.16	2.65	5.39	4.98
SrF_2	1.34	39.81	44.71	29.24	--	--	--
ThF_4	1.49	2.86	1.65	3.58	4.43	2.76	3.59

* ON CaF_2 THE GROWTH RATE OF PbF_2 ON (110) > (111) > (100), WHILE ON SrF_2, (110) ≥ (100) > (111).

** COATINGS ON ALL SUBSTRATES EMPLOYED CERAC RAW MATERIAL. GROWTH RATES OF ThF_4 ARE INDISTINGUISHABLE ON THE THREE ORIENTATIONS OF TWO SUBSTRATE MATERIALS.

TABLE 22. ABSORPTION COEFFICIENTS OF OXIDE, SULFIDE, AND SELENIDE COATING MATERIALS MEASURED BY DF LASER CALORIMETRY ON COATINGS OF HALF-WAVE OPTICAL THICKNESS AT A DESIGN WAVELENGTH OF 3.8 μm.

COATING MATERIAL	REFRACTIVE INDEX	COATING ABSORPTION COEFFICIENT, β (cm^{-1}), CaF_2 SUBSTRATE (100)	(110)	(111)	SrF_2 SUBSTRATE (100)	(110)	(111)
Al_2O_3	1.57	40.75	37.70	29.65	45.13	43.90	32.71
MgO	1.63	65.91	86.14	79.06	62.55	100.85	102.03
SiO	1.73	2.05	2.40	2.11	3.67	5.74	2.22
ZnSe	2.42				1.08	3.73	4.69
ZnS	2.23	10.10	8.81	10.20	16.73	13.52	19.61

Al_2O_3: ON BOTH SUBSTRATE MATERIALS THE GROWTH RATE ON (100) ≅ (110) > (111).

MgO: REFRACTIVE INDEX GIVEN FOR COATINGS ON CaF_2; ON SrF_2 $n(100) = 1.62$, $n(110) = 1.66$, $n(111) = 1.65$. ON CaF_2, THE GROWTH RATE ON (100) > (110) ≅ (111), WHILE ON SrF_2, (110) ≥ (111) > (100).

SiO: ON CaF_2, THE GROWTH RATE ON (100) > (111) > (110), WHILE ON SrF_2, (110) ≅ (111) > (100).

ZnSe: ON CaF_2, THE GROWTH RATE ON (100) ≅ (110) > (111), WHILE ON SrF_2, (110) ≅ (111) > (100).

ZnS: ON CaF_2, THE GROWTH RATE ON (110) > (100) > (111), WHILE ON SrF_2, (110) > (111) > (100).

TABLE 23. ABSORPTION COEFFICIENTS OF FLUORIDE COATING MATERIALS MEASURED BY CO LASER CALORIMETRY ON COATINGS OF HALFWAVE OPTICAL THICKNESS AT A DESIGN WAVELENGTH OF 5.3 μm.

COATING MATERIAL	REFRACTIVE INDEX	COATING ABSORPTION COEFFICIENT, β (cm^{-1})					
		CaF_2 SUBSTRATE			SrF_2 SUBSTRATE		
		(100)	(110)	(111)	(100)	(110)	(111)
PbF_2*	1.72	1.69	2.14	3.34	--	--	--
SrF_2	1.33	17.67	16.16	13.41	--	--	--
ThF_4**	1.48	3.24	3.11	2.98	1.41	0.78	0.78

* THE GROWTH RATE OF PbF_2 ON (110) > (111) > (110).

** COATINGS ON CaF_2 SUBSTRATES UTILIZED CERAC RAW MATERIAL; THOSE ON SrF_2 EMPLOYED BALZERS MATERIAL. GROWTH RATES ARE INDISTINGUISHABLE ON THE THREE ORIENTATIONS OF TWO SUBSTRATE MATERIALS.

TABLE 24. ABSORPTION COEFFICIENTS OF OXIDE, SELENIDE, AND SULFIDE COATING MATERIALS MEASURED BY CO LASER CALORIMETRY ON COATINGS OF HALF-WAVE OPTICAL THICKNESS AT A DESIGN WAVELENGTH OF 5.3 μm.

COATING MATERIAL	REFRACTIVE INDEX	COATING ABSORPTION COEFFICIENT, β (cm^{-1})					
		CaF_2 SUBSTRATE			SrF_2 SUBSTRATE		
		(100)	(110)	(111)	(100)	(110)	(111)
SiO	1.78	38.59	41.17	39.16	--	--	--
ZnSe	2.41	3.98	0.96	1.69	1.76	2.10	2.04
Zns	2.22	9.65	11.49	10.94	6.68	6.85	8.26

SiO: THE GROWTH RATE ON (100) > (110) ≅ (111).

ZnSe: ON CaF_2, THE GROWTH RATE ON (100) ≅ (110) > (111), WHILE ON SrF_2, (110) ≅ (111) > (100).

ZnS: ON CaF_2, THE GROWTH RATE ON (110) > (100) > (111), WHILE ON SrF_2, (110) > (111) > (100).

NORTHROP
Research and Technology Center

the results will vary. The error in the coating absorption determination for the low absorption group is of the order of 10 to 15%; that for the intermediate and high absorption groups is 3 to 5%.

In general, differences among materials are greater than differences among substrate orientations for the same coating material. However, differences among substrate orientations for the same coating may amount to factors of 2 to 4 (e.g. ZnSe on SrF_2 at 3.8 μm, Table 22, or on CaF_2 at 5.3 μm, Table 24). Structural and growth rate data are now available for establishing correlations among these properties. This will be carried out during the final phase of the effort.

5. FUTURE PLANS

The most critical tasks required to complete the contract include:

(1) βL vs. L measurements on PbF_2, ThF_4, and SiO films for halfwave, fullwave, and one and one-half wave thicknesses at 3.8 μm;

(2) Optimization of deposition conditions for ZnS and ZnSe;

(3) Deposition and characterization of AR coatings on single and polycrystalline substrates;

(4) Tests to establish the tolerance of Al_2O_3, PbF_2, ThF_4, ZnS, and ZnSe films to an HF environment.

(1), (3), and (4) have been initiated at this point in time. A first round of βL vs. L measurements has been carried out with PbF_2 films on CaF_2 (111) substrates at a design wavelength of 5.3 μm. These experiments yielded a β value of 0.26 cm^{-1} for the coating material and an absorptance of $\sim 1 \times 10^{-4}$ for the "coated surface" of the substrate.

This β is quite encouraging and the technique shows promise for isolating the absorptance of the coating material itself from that of the substrate/coating interface and the coating/air interface. Hence, we plan to carry out such measurements for three of the most promising coating materials deposited on three substrate orientations.

Three samples comprising ThF_4/SiO AR coatings on single crystal CaF_2 substrates 1.52 in. in diameter have been fabricated, characterized, and submitted to John Detrio of UDRI for damage testing. Fabrication and characterization of other designs on single and polycrystalline substrates will continue in the final phase of the effort.

REFERENCES

1. G. Hass, and E. Ritter, "Optical Film Materials and Their Applications", J. Vac. Sci. and Tech., Vol. 4, p. 71 (1966).

2. J. F. Hall and W. F. C. Ferguson, "Optical Properties of Cadmium Sulfide and Zinc Sulfide from 0.6 Microns to 14 Microns", JOSA, Vol. 45, p. 714 (1955).

3. R. J. Mattauch, "A Simple Vacuum Substrate Heater", Rev. Sci. Inst., Vol. 43, p. 148 (1972).

4. M. M. Hanson, P. E. Oberg, and C. H. Tolman, "Substrate-Temperature Measurement and Control", J. Vac. Sci. and Tech., Vol. 3, p. 277 (1966).

5. G. Hass and C. D. Salzberg, "Optical Properties of Silicon Monoxide in the Wavelength Region from 0.24 to 14.0 Microns", JOSA, Vol. 44, p. 181 (1954).

6. W. Steckelmacher, in Thin Film Microelectronics, L. Holland, Editor, p. 193, John Wiley & Sons, Inc., New York (1965).

7. K. H. Behrndt, in Physics of Thin Films, G. Hass and R. E. Thun, Editors, Vol. 3, p. 1, Academic Press, New York (1966).

8. L. Holland, Vacuum Deposition of Thin Films, Chap. 3, Chapman and Hall, London (1956).

9. R. W. G. Wyckoff, Crystal Structures, 2nd ed. Vol. 2, Wiley, N.Y. (1964).

10. R. W. G. Wyckoff, Crystal Structures, 2nd ed. Vol. 1, Wiley, N.Y. (1963).

11. ASTM Powder Diffraction File: Card No. 6-0290.

12. ASTM Powder Diffraction File: Card No. 16-160.

13. S. J. Holmes and P. Kraatz, "Investigation of Crystal Orientation Influence on Thin Film Coatings for CaF_2 Laser Windows" AFML Technical Report TR-75-188, Air Force Materials Laboratory, Wright-Patterson Air Force Base, Ohio 45433, (1965).

REFERENCES (cont'd)

14. ASTM Powder Diffraction File Card Nos. 23-1423 and 23-1426.

15. M. O. Aboelfotoh, K. C. Park, and W. A. Pliskin, "Infrared and high-energy electron diffraction analyses of electron-beam-evaporated MgO films" J. Appl. Phys. V. 48, pp. 2910-2917, 1977.

16. ASTM Powder Diffraction File Card No. 4-0829

17. " " " " " No. 7-239

18. " " " " " No. 19-771

19. " " " " " No. 4-0770

20. ASTM Powder Diffraction File Card Nos. 18-1170, 14-260.

21. " " " " " No. 5-0565

22. " " " " " No. 5-0522

23. " " " " " No. 15-105

24. " " " " " Nos. 5-492, 5-566.

25. " " " " " No. 12-688

26. A. R. Verma and P. Krishna, "Polymorphism and Polytypism in Crystals" Wiley, NY, 1966.

27. ASTM Powder Diffraction File Card No. 20-1437.

28. " " " " " No. 4-0864.

29. " " " " " No. 6-0262.

30. R. Weil, "Calculations of Small Absorption Coefficients From Calorimetric Experimental Data", Appl. Phys., Vol. 41, p. 3012, (1970).

31. J. S. Loomis, "Absorption in Coated Laser Windows", Appl. Opt. Vol. 12, p. 877, (1973).

32. P. Kraatz, and P. J. Mendoza, "CO Laser Calorimetry for Surface and Coating Evaluation", Proc. Fourth Conf. on Infrared Laser Window Materials, p. 77, (1975).

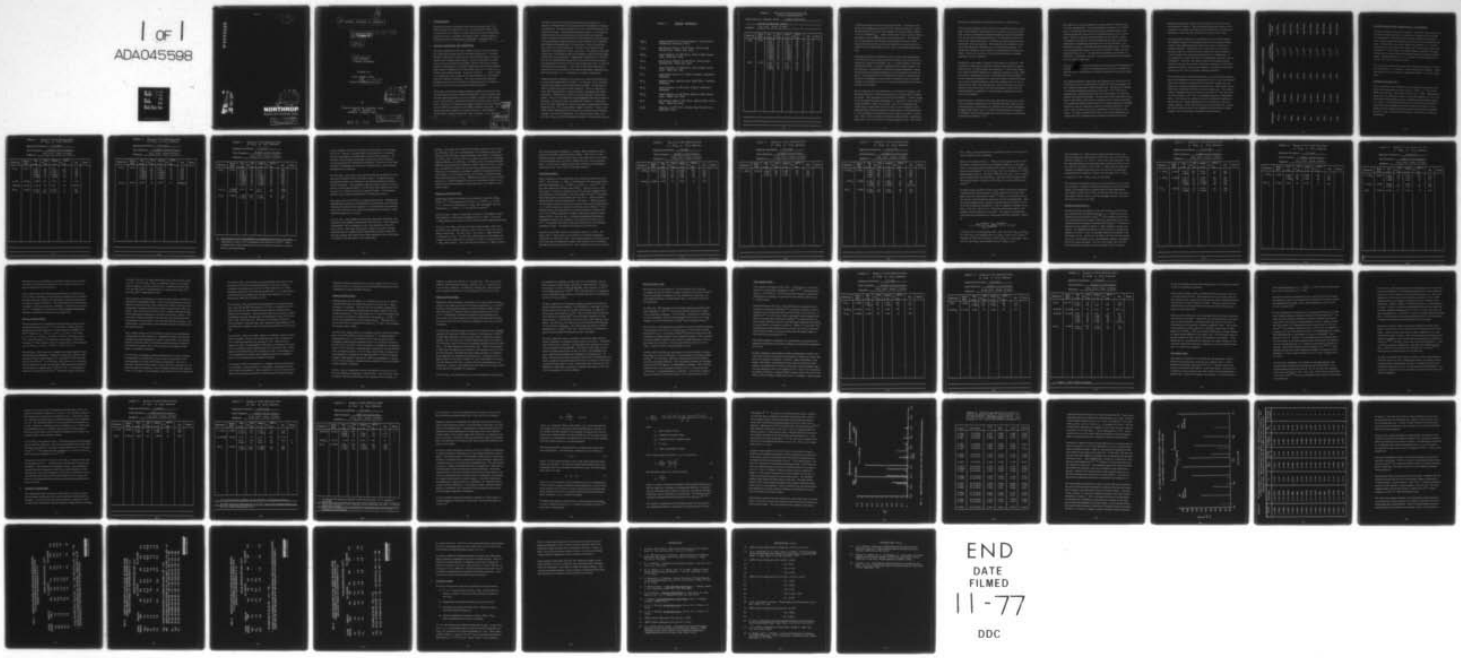
33. T. F. Deutsch, "Research in Optical Materials and Structures for High Power Lasers", Final Technical Report, Raytheon Research Division, ARPA Order 1180 (1973).

34. Kraatz, P., Holmes, S. J., and Klugman, A., "Absorptance of Coated Alkaline Earth Fluoride Windows at CO Laser Wavelengths", Proc. Fifth Conf. on IR Laser Window Materials, DARPA, (1975).

35. Loomis, J. S., "Computing the Optical Properties of Multilayer Coatings", Air Force Weapons Laboratory Technical Report No. AFWL-TR-75-202, September, 1975.

AD-A045 598 NORTHROP RESEARCH AND TECHNOLOGY CENTER HAWTHORNE CALIF F/G 11/3
OPTICAL COATINGS 2-6 MICRONS.(U)
SEP 77 P KRAATZ N00123-76-C-1321
UNCLASSIFIED NL

1 OF 1
ADA045598



END
DATE FILMED
11-77
DDC

AD A045598

AD No.
DDC FILE COPY

DDC
RECEIVED
OCT 27 1977
A

NORTHROP

Research and Technology Center

DISTRIBUTION STATEMENT A
Approved for public release;
Distribution Unlimited

(19)

(6) OPTICAL COATINGS 2-6 MICRONS.

(9) Technical Report. Jan-Jun 77

(11) September 1977

(12) 63p.

(10) P. Kraatz
Principal Investigator

Prepared For

Naval Weapons Center

(15) Contract No. N00123-76-C-1321

DDC
RECEIVED
OCT 27 1977
A

By

Northrop Research and Technology Center
3401 W. Broadway
Hawthorne, California 90250

DISTRIBUTION STATEMENT A
Approved for public release;
Distribution Unlimited

407696

4B

1. INTRODUCTION

Progress during the second half-year (January through June, 1977) under Contract No. N00123-76-C-1321 is reported here. The report is divided into four sections covering coating materials and deposition, coating structure, orientation, and growth rates, coating properties (refractive indices and absorption coefficients), and future plans. The materials include sapphire; fluorides of lanthanum, lead, *

2. COATING MATERIALS AND DEPOSITION

Successful deposition of thin film coatings requires careful control of the evaporation technique and the associated parameters. Currently, thermal evaporation in a high vacuum is the technique that is most frequently used to deposit film coatings. Thermal evaporation in a high vacuum has been extensively developed, and two of the most common modes of evaporation are resistance heating and electron-beam heating. Both modes of evaporation are widely used, and it is relatively easy to produce good optical coatings. In spite of this favor[illegible]spect, results of investigations of the properties of evaporated films have not always shown the expected consistency. The cause of these discrepancies probably does not lie in the method of evaporation itself, but rather in the lack of control of the many experimental parameters.

The quality of the optical coating materials depends on the purity of the starting materials and the method of preparation. Since impurities can increase optical absorption as well as initiate a variety of macroscopic or structural defects, commercial materials of highest purity must be used. The purity is frequently given in percentage of the main material, up to 99.9999%; the remainder consisting of unknown impurities. Although this number indicates ultrapure material, it still contains a great number of impurity atoms per cubic centimeter. It is, therefore,

* magnesium, strontium, thorium; silicon oxide, magnesium oxide; zinc sulfide, zinc selenide; lanthanum oxyfluoride.

Ltr on file
DISTRIBUTION/AVAILABILITY CODES
Dist. AVAIL. and/or SPECIAL
A

necessary to know the kind and concentration of all impurities. A variety of methods exist for the detection and determination of impurity concentration. The most important are x-ray, optical absorption, and mass spectroscopy. Knowing the impurities present, it is essential to determine which ones actually influence the respective properties. These impurities must be removed or at least reduced in concentration. Coating materials of desired purity are only available when a material has attained broad application. In most cases, it has to be purified; this is quite an involved operation. Drying is very essential if the material is contaminated by water in any form. The effects of absorbed moisture are so pronounced that they completely mask the normal aging and the basic loss mechanism. Adsorbed or trapped water or hydroxyl ions can be eliminated by drying under vacuum and slowly increasing the temperature to the level at which the loosely bound water is removed by diffusion and evaporation. True oxide or hydroxide compounds in solid form are not removable by this means, but require chemical reaction in some form, (i.e., scavenging by a reactive atmosphere).

Coating materials employed in the program are listed and identified as to source and nominal purity in Table 1. In all cases, these materials represent the highest purity commercially available. No attempt was made to further purify any of these materials. All were subjected to x-ray diffraction analysis to determine phase composition and identify impurities. Results were reported in the first quarterly report (September, 1976), for all materials except Lanthanum Fluoride and Silicon Monoxide. Results for LaF_3 are presented in Table 2. In this table, the first column identifies the material and phase determinable from the diffraction line. The second column, headed "Card Ref." refers to the ASTM Powder Diffraction File Card on which the data for the material or phase in question are tabulated. The columns headed "Obs. d(Å)" and "Obs. I/I_{100}" give the interplanar spacing in Å and relative intensity

TABLE 1. COATING MATERIALS

Al_2O_3	Random Chunks of UV-Grade Sapphire, Union Carbide Corporation, San Diego, Calif.
LaF_3	Hot-Pressed Tablets, 99.9% Purity, Balzers High Vacuum Corp., Santa, Ana, Calif.
MgF_2	Fused Granules, 99.99% Purity, Balzers High Vacuum Corp., Santa Ana, Calif.
MgO	Hot-Pressed Tablets, 99.95% Purity, Balzers High Vacuum Corp., Santa Ana, Calif.
PbF_2	Fused Granules, 99.99% Purity, Balzers High Vacuum Corp., Santa Ana, Calif.
SiO	Linde Select Grade, R. D. Mathis Company, Long Beach, California.
SrF_2	Random Chunks, Optical Grade, EMCO Sales, Anaheim, California.
ThF_4	Fused Granules, 99.9% Purity, CERAC, Milwaukee, Wisconsin.
ThF_4	Fused Granules, 99.9% Purity, Balzers, High Vacuum Corp., Santa, Ana, Calif.
ZnS	Hot-Pressed Tablets, 99% Purity, Balzers High Vacuum Corp., Santa Ana, Calif.
ZnSe	Granules, 99.99% Purity, Balzers High Vacuum Corp., Santa Ana, Calif.

TABLE 2 . Results of X-Ray Diffraction Study of LaF_3 Coating Material.

Material Source, Condition, Purity : Balzers Ch72-390/3 (99.9%) As Received, Ground.

Radiation : CuK_α 35 kV. 18 mA. Ni Filter

Material	Card Ref.	Obs d (Å)	Obs I/I_{100}	ASTM d (Å)	ASTM I/I_{100}	hkl	Notes
LaF_3	8-461	3.667	32	3.67	40	002	
		3.580	19	3.59	32	110	
		3.218	59	3.229	100	111	
		2.5615	07	2.569	11	112	
		2.0213	43	2.025	54	113	
		1.8024	27	1.8064	33	302	
		1.7477	27	1.7451	20	221	
		1.4455	08	1.4487	14	223	
		1.3346	19	1.3354	15	411	
		1.1872	14	1.1877	14	413	
LaOF	5-0470	3.348	100	3.35	100	101	
		2.905	22	2.90	25	110	
		2.0606	46	2.06	60	112	
		1.7634	22	1.76	22	103	

of diffraction peaks observed in the present study. To facilitate comparison and emphasize pecularities of the evaporant material, the Powder Diffraction File data are also tabulated in columns headed "ASTM d (Å)" and "ASTM I/I_{100}". Miller indices (hkl) of the respective diffracting planes are also tabulated when given on the cards. The main feature of this analysis worth noting is that diffraction lines for LaOF (which should be present only in trace amounts as an impurity) are as intense or more intense than those for LaF_3, the nominal coating material.

Although the intensity of diffracted x-rays is not simply proportional to the amount of a given phase present in a sample (due to losses from absorption, preferred orientation, etc.), such high relative intensities indicate that LaOF is a major constituent of the coating material. If this material is redeposited on substrates during evaporation, coating inhomogeneities and high absorptance in the mid-infrared would be expected. The redeposition of this material in addition to oxides and hydroxides of Lanthanam is in fact found in conjunction with a very high absorption coefficient at 3.8 μm, as will be demonstrated in successive sections of this report.

Silicon monoxide was also subjected to x-ray diffraction analysis, with the expectation that it would be amorphous to x-ray and show no diffraction peaks. This expectation was very nearly fulfilled. A single, broad, very weak diffraction peak attributable to α quartz (101) with a spacing of approximately 3.348Å was detected. This is not unexpected and should cause no particular concern for the 3.8 μm wavelength region. Although SiO_2 itself is not especially detrimental to coating absorption in the mid infrared, its tendency to act as a getter for water is a problem. Thus, a film consisting of SiO and redeposited SiO_2 could absorb heavily at 5.3 μm or 2.7 μm if it contained trapped water. This will be

discussed in connection with absorption results in a later section.

In the vacuum deposition of thin films by an evaporation process, knowledge of the substrate temperature and its control is often very important. In fact, the substrate temperature plays an especially important role for the whole condensation process. It controls the surface mobility of the condensing atoms or molecules and determines the degree of disorder of the growing film. Film adhesion and durability are improved by heating the substrates prior to and during deposition. Of paramount importance is the removal of adsorbed gases from the substrate. Thus water removal is one of the main reasons for heating substrates prior to deposition.

In practice a wide range of substrate temperatures is employed. The deposition of metal oxides requires substrate temperatures of approximately 300°C to obtain optimal film properties.[1] On the other hand, zinc sulfide should be deposited at a substrate temperature below 180°C to provide a compromise between reevaporation and film durability.[2] If a low substrate temperature is required to obtain a desired film property such as minimal scattering, and if this temperature is too low to remove water vapor from the substrate, then the substrate can be preheated to remove the water vapor and subsequently cooled to the required deposition temperature. Glow discharge cleaning can also be used in this situation.

Since the index of refraction of the films and film structure are a function of substrate temperature, it is important that both substrates and monitoring pieces be maintained at a uniform and constant temperature throughout the deposit cycle. A typical substrate heater is described by Mattauch[3] and the measurement and control of substrate temperature is discussed by Hanson, et al.[4]

The objective in vacuum evaporation is nearly always to deposit films to certain specifications. If the specification is primarily one of thickness, it is sufficient to determine when the accumulated deposit has reached the desired value so that the deposition process can be terminated. However, intensive film properties such as density, stress, crystallinity, and index of refraction depend on the rates at which the evaporant and residual gas molecules arrive at the substrate. It is therefore necessary to maintain specified evaporation rates. The influence of the deposition rates on the index of refraction of SiO has been studied by Hass, et. al.[5] A high rate of deposition corresponds to a high index of refraction, whereas, a slow rate of deposition corresponds to a low index of refraction.

Reviews of thickness and rate monitors have been given by Steckelmacher[6] and Behrndt. The control of evaporation rate is a more complex task than thickness control because it requires adjustment of the source temperature.

All coating depositions required for this program were carried out in a commercial vacuum system (Balzers Model 710) which is equipped with an oil diffusion pump and a liquid nitrogen trap. This system is capable of routinely maintaining pressures of the order of 10^{-6} Torr and is equipped with a substrate heater and a thin film monitor to control deposition rate and film thickness. Proper control of the thickness of each layer is afforded by observing the reflectance at the control wavelength of a suitably positioned monitor plate in the coating chamber and stopping deposition when the reflectance reaches a predetermined level. In all cases, care is taken to ensure the uniformity of the thickness of the layers. In order to obtain uniform layers, the window substrates are rotated above the evaporation source during the deposition process.

Deposition parameters utilized in this program are summarized for each material in Table 3. Electron beam heating was employed in the evaporation of slightly more than half of the materials, while thermal evaporation from a boat was utilized in the balance of the cases.

Clean substrate surfaces are a prerequisite for successful coatings. The slightest amount of contamination can cause an immense amount of harm in the coating deposition process as well as an increase in surface absorption. Cleaning is an art rather than a science and, therefore, there is a great diversity of opinion on what constitutes a "good" procedure for cleaning substrates prior to coating them. A full treatment of various methods for cleaning glass substrates is given by Holland.[8] However, the sensitive nature of the highly polished surfaces of the fluoride windows requires the avoidance of such harsh cleaning procedures, since serious damage to the delicate optical surfaces can be the result of improper cleaning techniques.

The cleaning process utilized at Northrop to clean the fluoride windows prior to the deposition of the coating has been more or less conventional. Before the windows are placed into the system for coating, they are cleaned in a solution of detergent and warm water, then rinsed with distilled water and alcohol and blown dry with nitrogen gas. The coating system is pumped down to a pressure of less than 10^{-6} Torr and a pressure of less than 5×10^{-6} Torr is maintained during the coating deposition. The windows are heated to the desired substrate temperature and just prior to coating deposition they are subjected to a glow discharge cleaning. So far this procedure has been adequate for cleaning the fluoride surfaces prior to the deposition of antireflection coating designs, and for calorimetric absorption measurements.

TABLE 3. DEPOSITION PARAMETERS

MATERIAL	METHOD OF EVAPORATION	SUBSTRATE TEMPERATURE	DEPOSITION PRESSURE (TORR)	DEPOSITION RATE
Al_2O_3	E-Beam	200°C	5×10^{-5}	~600 Å/Min
LaF_3	Mo Boat	200°C	8×10^{-6}	~1800 Å/Min
MgF_2	E-Beam	200°C	2×10^{-6}	~1800 Å/Min
MgO	E-Beam	200°C	6×10^{-5}	~1200 Å/Min
PbF_2	E-Beam	200°C	7×10^{-6}	~1800 Å/Min
SiO	Ta Boat	200°C	$<1 \times 10^{-6}$	~3000 Å/Min
SrF_2	Mo Boat	200°C	8×10^{-6}	~1800 Å/Min
ThF_4	E-Beam	200°C	4×10^{-6}	~1800 Å/Min
ZnS	Ta Boat	150°C	8×10^{-6}	~1800 Å/Min
ZnSe	Ta Boat	150°C	4×10^{-6}	~1800 Å/Min

3. COATING STRUCTURE, ORIENTATION, AND GROWTH.

Crystal structures, preferred orientation, and growth characteristics of thin films investigated under this contract are detailed in this section. X-ray diffraction, utilizing a General Electric XRD-6 diffractometer with a copper-target tube operated at 35kV and 18 mA, provided the raw data. A nickel filter was used to obtain CuK_α radiation (λ = 1.5405 Å). Patterns were taken using a scan speed of 2° (2θ) per minute and a time constant of 0.5 in all cases, slit widths, detector sensitivity, and gain settings were varied as required to obtain optimum resolution and peak height. Tabulated values of d vs. 2θ obtained from the Bragg law, $n\lambda = 2d \sin\theta$, were used to reduce the data.

The thin film materials are grouped and discussed on the basis of chemical composition, i.e. fluorides, oxides, selenides and sulfides. Within each group, they are arranged in alphabetical order, i.e. LaF_3, MgF_2, PbF_2, ...

Lanthanum Fluoride, LaF_3 –

LaF_3 crystallizes in the hexagonal system with space group $P6_3/mmc$; the unit cell dimensions are given as a_o = 7.184Å, c_o = 7.351 on the ASTM card (#8-461), while Wyckoff[9] gives a_o = 3.148Å. Experimental results of x-ray diffraction scans of LaF_3 films (halfwave at 3.8 μm) on three different orientations of CaF_2 substrates are presented in tables 4, 5, and 6. Two salient features of these results are the moderate to strong preferred orientation in the films with some evidence of correlation with the substrate orientation and the strong peaks attributable to LaOF, La_2O_3, and LaO OH occurring on (100) and (111) substrate orientations.

TABLE 4. Results of X-Ray Diffraction Study of LaF_3 on CaF_2 Substrate.

Substrate Orientation: 1° Λ (100)

Film Thickness: 12,500 Å ($\lambda/2$ at 3.8 μm)

Radiation: CuK_α 35 kV. 18 mA. Ni Filter

Material	Card Ref.	Obs d (Å)	Obs I/I 100	ASTM d (Å)	ASTM I/I 100	hkl	Notes
LaF_3	8-461	3.587	03	3.59	32	110	
		3.223	08	3.229	100	111	
		2.070	03	2.075	51	300	
		1.8024	04	1.8064	33	302	
		1.0066	04	1.0078	03	117	
La OF	6-0281	1.5087	100	1.503	05	432	
LaO OH	19-656	3.015	02	3.04	60	$10\bar{2}$, 002	
CaF_2	4-0864	2.724	63	2.732	--	200	
		1.3633	>100	1.366	12	400	

TABLE 5. Results of X-Ray Diffraction Study of LaF_3 on CaF_2 Substrate.

Substrate Orientation: 3° Λ (110)

Film Thickness: 12,500 Å (λ/2 at 3.8 μm)

Radiation: CuK_α 35 kV. 18 mA. Ni Filter

Material	Card Ref.	Obs d (Å)	Obs I/I 100	ASTM d (Å)	ASTM I/I 100	hkl	Notes
LaF_3	8-461	3.587	02	3.59	32	110	
		2.067	100	2.075	51	300	
		1.8057	26	1.8064	33	302	
		1.3329	03	1.3354	15	411	
		1.1872	02	1.1877	14	413	
		1.0357	03	1.0370	03	600	
La_2O_3	22-641	2.293	04	2.298	04	$20\bar{4}, \bar{5}03$	

TABLE 6. Results of X-Ray Diffraction Study of LaF_3 on CaF_2 Substrate.

Substrate Orientation: 1° Λ (111)

Film Thickness: 12,500 Å ($\lambda/2$ at 3.8 μm)

Radiation: CuK_α 35 kV. 18 mA. Ni Filter

Material	Card Ref.	Obs d (Å)	Obs I/I 100	ASTM d (Å)	ASTM I/I 100	hkl	Notes
LaF_3	8-461	3.672	76	3.67	40	002	
		3.580	18	3.59	32	110	
		2.070	04	2.075	51	300	
		1.8364	10	1.8377	05	004	
		1.8024	03	1.8064	33	302	
		1.7400	06	1.7451	20	221	
		1.2239	03	1.2254	02	006	
		1.619	01	1.1601	02	116	
La_2O_3	5-0602	3.477	100	3.41	34	100	1
	24-554			3.51	30	100	
CaF_2	4-0864	3.1399	>100	3.153	94	111	
		1.5751	28	1.5765	--	222	

1. The spacing of 3.41 Å corresponds to a hexagonal form of La_2O_3 at room temperature, while 3.51 Å was obtained on the material at 2100° C. Hence, it appears that a high temperature form of the oxide is quenched in the thin film at room temperature.

If LaF_3 exhibits a preferred orientation on (100) CaF_2, it would appear to be (111). However, the other peaks of near half the (111) intensity indicate a high degree of randomness in the thin film orientation. On the other hand the single strong peak arising from LaOF indicates a very strong preferred orientation in that phase. The source of the latter material is undoubtedly the coating raw material itself, which contains an abundance of it (table 2).

On (110) CaF_2, LaF_3 shows a strong (100) preferred orientation as indicated by the intensity of the (300) peak in table 5. It appears that an appreciable fraction of crystallites in the coating material have taken a (302) orientation. The interplanar spacing of LaF_3 in these two orientations is within approximately 7% of the CaF_2 (220) spacing in the (110) direction (i. e. normal to the [110] substrate surface). This indicates influence of the coating orientation by the substrate structure.

The La_2O_3 peak on (110) CaF_2 is not particularly strong. Although substantially equal quantities of contaminants should deposit on all substrate orientations in films of this thickness, it is possible that the crystallite size of this material is very small and orientation near random, so that diffraction peaks are very weak.

On (111) CaF_2, LaF_3 exhibits a strong (001) preferred orientation, with a minority of crystallites oriented near (100) and (110). This orientation of (hexagonal) LaF_3 corresponds to the 3-fold symmetry of the (111) CaF_2 surface. The single La_2O_3 peak is again very strong, showing marked preferred orientation and an appreciable quantity of material. The large spacing may indicate that a high temperature form of the oxide is quenched in the thin film at room temperature.

On SrF_2, LaF_3 films show preferred orientation similar to that on CaF_2. On (100) SrF_2, LaF_3 has a predominantly (111) orientation with strong (100) and (110) type peaks, again indicating a high degree of randomness as on CaF_2 (100). On SrF_2 (110), LaF_3 shows a strong (110) orientation, unlike its behavior on (110) CaF_2. La $(OH)_3$ shows one strong peak (201), indicating strong preferred orientation of this impurity on (110). In addition, the patterns for both (110) and (111) SrF_2 substrates indicate significant microcrystalline or amorphous material with spacings in the 4 to 6Å region. The orientation of LaF_3 on (111) SrF_2 is again the basal (001) orientation shown on CaF_2. Relative growth rates of LaF_3 on CaF_2 and SrF_2 are indistinguishable for the three orientations studied, as reported in the previous quarterly report dated May, 1977 (figures 1 and 2 of that report).

Magnesium Fluoride, MgF_2 –

Magnesium Fluoride crystallizes in the tetragonal cassiterite (SnO_2) structure[10, 11] with space group $P4/mnm$, $a_o = 4.623$Å, $c_o = 3.052$Å, $Z = 2$. Another form designated α - MgF_2, also tetragonal, with cell dimensions $a_o = 9.927$Å $c_o = 6.172$Å has been reported[12].

On CaF_2 (100), it takes a strong (001) orientation, with slightly smaller (002) spacing (1.511Å) than the tabulated value of 1.526Å. Very weak α- MgF_2 (440) and (216) lines are also observed with the tabulated spacings.

On CaF_2 (110), MgF_2 (211) and (112) have equal intensity, while (110) has 70% of this maximum intensity. Hence, this is a more or less randomly oriented film. On CaF_2 (111), a very weak α - MgF_2 (800) line is observed at 1.161Å. The only other diffraction line in the pattern not arising from the substrate has a spacing of 3.477Å, or three times the α- MgF_2 (800) spacing. This may indicate a distorted α - MgF_2 structure

with strong preferred orientation. On SrF_2, MgF_2 coatings are highly stressed and exhibit crazing and other defects. They show no X-ray diffraction peaks, indicating either that no long range order is developed or that crystallites are too small to diffract X-rays to yield significant peaks. Growth rates of MgF_2 on both CaF_2 and SrF_2 are indistinguishable among (100), (110), and (111) substrate surfaces.

Lead Fluoride PbF_2 -

PbF_2 crystallizes in two polymorphs with a transition temperature near 250°C. One of these, α - PbF_2, is orthorhombic with space group Pbnm, and lattice parameters $a_o = 7.357\text{Å}$, $b_o = 4269\text{Å}$, $c_o = 3.891\text{Å}$.[10] The unit cell contains four formula units of PbF_2. This structure is of the $PbCl_2$ type, in essence a distorted cubic close packing of halogen atoms with lead atoms accommodated in the same plane with them[10]; this phase has a higher atomic packing density than the cubic β - phase and hence should be stable at lower temperatures. The cubic β - PbF_2 polymorph has the fluorite structure with space group Fm3m and unit cell dimension $a_o = 5.927\text{Å}$; the unit cell contains four formula units of PbF_2.[10] It was found previously that both phases occurred in quarterwave thicknesses (at 5.3 μm) of PbF_2 deposited on single crystal CaF_2 substrates maintained at 200°C, with the cubic β - phase predominating and taking an orientation parallel to the substrate, with a mismatch of the order of 8%.[13] The growth rate of these films was found to vary with substrate orientation, being ~ 3% faster on (110) than on (100) and (111).

Results of the present work are presented in tables 7, 8, and 9. On CaF_2 (100), β - PbF_2 takes a very strong (111) preferred orientation, with minor (331) and (511) lines. This contrasts sharply with the previous X-ray and electron diffraction results, which showed a (100) orientation throughout the bulk of the film and a (110) orientation near the free surface.

TABLE 7. Results of X-Ray Diffraction Study of PbF_2 on CaF_2 Substrate.

Substrate Orientation: 1° Λ (100)

Film Thickness: 10,900 Å (λ /2 at 3.8 μm)

Radiation: CuK_α 35 kV. 18 mA. Ni Filter

Material	Card Ref.	Obs d (Å)	Obs I/I 100	ASTM d (Å)	ASTM I/I 100	hkl	Notes
β - PbF_2	6-0251	3.424	100	3.428	100	111	
		1.714	11	1.715	14	222	
		1.363	05	1.362	27	331	
		1.143	< 01	1.143	20	511	
α - PbF_2	6-0288	3.782	01	3.824	10	002	

TABLE 8. Results of X-Ray Diffraction Study of PbF_2 on CaF_2 Substrate.

Substrate Orientation: 5° Λ (110)

Film Thickness: 10,980 Å ($\lambda/2$ at 3.8 μm)

Radiation: CuK_α 35 kV. 18 mA. Ni Filter

Material	Card Ref.	Obs d (Å)	Obs I/I 100	ASTM d (Å)	ASTM I/I 100	hkl	Notes
β - PbF_2	6-0251	3.424	100	3.428	100	111	
		2.097	98	2.100	73	220	
		1.711	06	1.715	14	222	

TABLE 9. Results of X-Ray Diffraction Study of PbF_2 on CaF_2 Substrate.

Substrate Orientation: 1.8° Λ (111)

Film Thickness: 10,980 Å (λ/2 at 3.8 μm)

Radiation: CuK_α 35 kV. 18 mA. Ni Filter

Material	Card Ref.	Obs d (Å)	Obs I/I 100	ASTM d (Å)	ASTM I/I 100	hkl	Notes
β- PbF_2	6-0251	3.424	100	3.428	100	111	
		1.714	29	1.715	14	222	
		1.306	<01	1.328	21	420	
		1.142	02	1.143	20	511	
α - PbF_2	6-0288	3.798	05	3.824	10	002	
		1.2798	<01	1.2854	05	143	
		1.2470	<01	1.2570	03	224, 311	
CaF_2	4-0814	3.156	09	3.153	94	111	
		1.0515	<01	1.0512	07	511	

The α- PbF_2 in the present study is oriented near (001); in the previous work it showed a (012) orientation.

On the (110) surface of CaF_2, β - PbF_2 is the only phase present, showing equally strong (110) and (111) orientations (Table 8). In previous work, a very strong (110) orientation with minor (111) and α- PbF_2 (103) lines was determined.[13] On (111) CaF_2, the (111) orientation of β- PbF_2 predominates (Table 9), with minor (420) and (511) lines. The α - phase takes a predominant (001) orientation, with minor lines of higher index. The general behavior of PbF_2 on (111) CaF_2 is in accord with previous results.[13]

Present results on relative growth rates of PbF_2 on the three substrate orientations show fastest growth on (110) followed by (111) and (100), again in accord with previous results.[13] Hence, it is difficult to reconcile structure and growth rate data in the two sets of experiments. Present results suggest that the preferred growth direction of PbF_2 is [111] on all three substrate orientations. This is mitigated somewhat on (110) CaF_2, where the (110) line of β - PbF_2 has an intensity equal to (111). Reasons for this behavior are not clear. The degree of mismatch between the lattice parameters of coating and substrate materials, defined as

$$\Delta d = \frac{d_{hkl}\,(\text{coating}) - d_{hkl}\,(\text{substrate})}{d_{hkl}\,(\text{substrate})} \times 100\,\%$$

is about 8.7% for corresponding (100), (110), and (111) CaF_2 and βPbF_2. On (110) CaF_2, the mismatch with (111) PbF_2 is only 8.8%, so the coexistence of (111) and (110) PbF_2 on (110) CaF_2 is not surprising. However on (100) CaF_2, the mismatch with (111) PbF_2 is 37%.

The orientation of β - PbF_2 films on SrF_2 substrates follows substrate orientations nearly perfectly in all three cases as indicated by the data of tables 10, 11, and 12. This is not at all surprising, since the mismatch between corresponding planes of PbF_2 and SrF_2 is 2.4% for (100) and (110) and 2.3% for (111). α - PbF_2 occurs on the (100) substrate orientation with about equal (010) and (012) orientations; mismatch with the substrate is about 13% while that with β - PbF_2 is about 10%. No α - PbF_2 occurs on (110) SrF_2.

The presence of lead oxide, Pb_2O_3 on (110) and PbO on (111), comes as no surprise. It tends to increase the refractive index of the films slightly, but probably does not appreciably increase absorptance. The relative growth rates of PbF_2 on (110) and (100) SrF_2 are essentially equal, with the rate on (110) being slightly greater. The slowest growth rate is on (111) SrF_2.

Strontium Fluoride (SrF_2).

Strontium fluoride crystallizes in the cubic fluorite structure with space group Fm3m and lattice parameter a_o = 5.800Å; the unit cell contains four formula units of SrF_2.[10] It was found previously that SrF_2 films deposited on single crystal CaF_2 substrates took on very strong preferred orientations following the substrate.[13] However, its behavior is very similar to that of β - PbF_2 deposited on CaF_2 substrates. For halfwave thicknesses of SrF_2 on CaF_2 at design wavelengths of 3.8 and 5.3 μm, the dominant preferred orientation in the thin films is (111). For the 5.3 μm films, (100) and (110) type peaks are of very low intensity on the corresponding substrate orientations, with (111) always strongest. For the 3.8 μm films, the (100) and (110)-type peaks are about twice the intensity of the (111) peaks.

TABLE 10. Results of X-Ray Diffraction Study of PbF_2 on SrF_2 Substrate.

Substrate Orientation: 2.5° Λ (100)

Film Thickness: 5,490 Å (λ /4 at 3.8 μm)

Radiation: CuK_α 35 kV. 18 mA. Ni Filter

Material	Card Ref.	Obs d (Å)	Obs I/I 100	ASTM d (Å)	ASTM I/I 100	hkl	Notes
β - PbF_2	6-0251	2.957	100	2.970	56	200	
		1.4816	35	1.485	10	400	
α - PbF_2	6-0288	3.276	02	3.290	100	012	
		3.201	01	3.222	40	020	
		1.6407	01	1.6445	13	024	
		1.6040	04	1.6101	04	040	
SrF_2	6-0262	2.891	53	2.900	25	200	
		1.4485	71	1.4499	15	400	

TABLE 11. Results of X-Ray Diffraction Study of PbF_2 on SrF_2 Substrate.

Substrate Orientation: 2° Λ (110)

Film Thickness: 5490 Å (λ/4 at 3.8 μm)

Radiation: CuK_α 35 kV. 18 mA Ni Filter

Material	Card Ref.	Obs d (Å)	Obs I/I 100	ASTM d (Å)	ASTM I/I 100	hkl	Notes
β - PbF_2	6-0251	3.424	06	3.428	100	111	
		2.095	100	2.100	73	220	
		1.0485	05	1.050	08	440	
Pb_2O_3	23-331	2.319	02	2.317	02	003	

TABLE 12. Results of X-Ray Diffraction Study of PbF_2 on SrF_2 Substrate.

Substrate Orientation: 0.5° Λ (111)

Film Thickness: 5490 Å (λ/4 at 3.8 μm)

Radiation: CuK_α 35 kV. 18 mA. Ni Filter

Material	Card Ref.	Obs d (Å)	Obs I/I 100	ASTM d (Å)	ASTM I/I 100	hkl	Notes
β - PbF_2	6-0251	3.418	100	3.428	100	111	
		1.7098	07	1.715	14	222	
		1.1406	01	1.143	20	511	
α - PbF_2	6-0288	3.782	03	3.824	10	002	
		1.8937	<01	1.912	16	004	
PbO	5-0561	2.506	<01	2.510	18	002	

Diffraction lines corresponding to elemental strontium and its oxides are found on all substrate orientations, but in greater numbers and greater intensities on (100) and (111).

Thus it appears that the preferred growth direction of SrF_2 films is [111] on CaF_2 substrates, but the substrate orientation has a variable influence upon this, possibly corresponding to substrate temperature or impurity content of the films. Non-stoichiometry and the presence of oxygen or hydroxyl groups are problematic, as observed in previous work.[13] No difference in growth rate of SrF_2 among the three CaF_2 substrate orientations was found in the present work.

Thorium Fluoride (ThF_4)

Thorium tetrafluoride crystallizes in the monoclinic system with the zirconium fluoride structure.[9] Two unit cells of slightly different dimensions have been reported in recent entries in the ASTM card file.[14] These are $a_o = 13\text{Å}$, $b_o = 11.1\text{Å}$, $c_o = 8.6\text{Å}$, $\beta = 126.0°$ and $a_o = 12.9\text{Å}$, $b_o = 10.93\text{Å}$, $c_o = 8.58\text{Å}$, $\beta = 126.4°$, with space group C 2/c and cell content Z = 12 formula units of ThF_4. In the older literature,[9] a body-centered cell (I 2/c) was chosen, with dimensions $a_o = 10.64\text{Å}$, $b_o = 11.0\text{Å}$, $c_o = 8.6\text{Å}$, $\beta = 94°50'$, Z = 12.

On (100) CaF_2, ThF_4 films are crystalline with nearly equal (270) and ($21\bar{3}$) preferred orientations. Mismatch of ThF_4 (270) with the (100) spacing of CaF_2 is approximately 11%; mismatch of ($21\bar{3}$) with (200) CaF_2 is less than 1%. On (110) CaF_2, ThF_4 films are microcrystalline (amorphous to X-ray) with subequal diffuse maxima in diffracted X-ray intensity at approximately 3.8Å and 2.01Å, corresponding respectively to ThF_4 (220) and (103).[14] Mismatch between ThF_4 (220)

and CaF_2 (110) is 1.6% while that between ThF_4 (103) and CaF_2 (220) is 4.8%. On (111) CaF_2, ThF_4 is crystalline, taking a very strong $(32\bar{1})$ orientation, with one weak (332) line. Mismatch between CaF_2 (111) and ThF_4 $(32\bar{1})$ is approximately 9%; that between ThF_4 (332) and CaF_2 (222) is approximately 10%.

These results are in general accord with previous work, but details of the preferred orientations differ. This is not surprising since overall behavior remains the same: ThF_4 films tend to adopt a preferred crystallographic orientation leading to minimal mismatch with a CaF_2 substrate. Since the structure of ThF_4 is more complex than that of CaF_2, several interplanar spacings may lie near a given CaF_2 spacing. The particular orientation adopted by the film may then depend upon other considerations than mismatch across the film-substrate interface, e.g. contaminants, stacking faults, and preferential growth directions in the film material itself.

ThF_4 coating material from two different vendors (Cerac and Balzers) was deposited on SrF_2 substrates. Although the number and intensity of diffraction peaks attributable to oxides, oxyfluorides, and hydrated fluorides of thorium differ in thin films deposited using raw material from different vendors, the overall structure and orientation of the films is remarkably consistent.

On (100) SrF_2 the strongest coating diffraction line for Cerac material is attributable to hydrated ThF_4 with an observed spacing of 3.20Å corresponding to a strong (132) preferred orientation. The line of secondary intensity is attributable to ThF_4 (252) with a spacing of 1.61Å. Minor amounts of amorphous or microcrystalline material with spacings in the 5 to 9Å region, corresponding to ThF_4 (200) and (110) are observed.

For Balzers ThF_4, the coating is microcrystalline with primary orientation near (512) with an observed spacing of 1.466Å and subequal secondary orientations near (103) (d = 2.004Å) and (220) (d = 3.80Å). Mismatch between the (512) spacing and (400) SrF_2 is 1%, that between (103) and (220) SrF_2 (exposed on the SrF_2 (100) surface) is 2%, and that between (220) and (111) SrF_2 is 13%.

On (110) SrF_2, ThF_4 comprises predominantly well crystallized material with a strong ($52\bar{1}$) orientation (d = 2.27Å), a mismatch of 10.7% with (220) SrF_2 for films fabricated using material manufactured by either Cerac or Balzers. Both materials show minor amounts of poorly crystallized thin film with spacings corresponding to ThF_4 ($31\bar{1}$), (220), (030), ($31\bar{2}$), ($32\bar{1}$) and (310). Evidence for a substantial amount of microcrystalline, hydrated ThF_4 with a spacing of approximately 3.48Å was observed in a pattern from one coating fabricated from Cerac material.

On (111) SrF_2, ThF_4 from either vendor is crystalline, taking a strong (030) orientation, with an observed spacing of 3.697Å, a mismatch of 10.3% with the substrate (111) spacing of 3.35Å. Material with a spacing of 1.85Å, corresponding to (322) ThF_4 is also observed, giving rise to a diffracted X-ray intensity about 25% of the (030) line. Minor amounts of hydrated ThF_4 with a spacing of 2.45Å, corresponding to a (151) orientation are found in films fabricated from Cerac material, but not in those fabricated from Balzers material.

In summary of ThF_4 characteristics, it appears that the material may be crystalline, microcrystalline, or amorphous, depending upon substrate type and orientation. When crystalline, it tends to take an orientation which minimizes mismatch with the fluoride substrate spacing.

Hydrated material in thin film form is more common when Cerac raw material is used. Growth rates are indistinguishable among the three orientations of either substrate material.

Aluminum Oxide (Al_2O_3).

Although Al_2O_3 may crystallize in a multiplicity of forms, we shall be concerned only with the common form known variously as α - Al_2O_3, corundum, or sapphire. The structure is most easily visualized as a hexagonal close-packing of oxygen ions with small metallic ions lying in some interstices.[9] The space group is R $\bar{3}$ c and the structure may be referred to a primitive rhombohedral cell having a_o = 5.128Å, α = 55°20' and containing two formula units of Al_2O_3.[9] Alternatively, it may be referred to a hexagonal cell having a_o = 3.763Å, and containing six formula units of Al_2O_3.

On (100) CaF_2, Al_2O_3 films are crystalline with the corundum structure and a very strong (018) preferred orientation.[15] A small amount of material takes a (1 2 10) orientation and a minor amount of microcrystalline material having spacings in the 3 to 5 Å region is observed. On (110) CaF_2, the film is microcrystalline or amorphous with spacings in the 1.8 to 2.1Å region, corresponding to spacings for several different forms of aluminum oxide. On (111) CaF_2, Al_2O_3 films are largely microcrystalline or amorphous with spacings in the 5.9 and 7.4Å regions. A single, sharp peak at a spacing of 3.497Å corresponding to α -Al_2O_3 (012) is of low intensity, indicating that crystallinity is poorly developed on this substrate orientation.

On SrF_2, Al_2O_3 is apparently entirely amorphous to X-rays on two of the three substrate orientations, (100) and (110). On (111) SrF_2, microcrystalline material predominates with a spacing in the 6Å region. In

addition, a single weak peak at 3.69Å is observed. This is not attributable to common phases of Al_2O_3, $Al(OH)_3$, AlF_3, or elemental Al, or to the SrF_2 substrate. On both CaF_2 and SrF_2 the relative growth rate of Al_2O_3 is slowest on (111) and equally fast on (100) and (110).

Magnesium Oxide (MgO).

Magnesium oxide (periclase) crystallizes in the cubic sodium chloride structure with space group Fm3m and lattice parameter a_o = 4.211Å.[10] Recently reported experimental work with thin films of MgO on amorphous substrates[15] indicates that the preferred growth direction is < 111 >, independent of substrate temperature and deposition rate. Our results on oriented single crystal CaF_2 substrates tend to confirm this for the (100) and (110) substrate orientations, but not for the (111) orientation.

On (100) CaF_2, MgO films take a strong (111) orientation with a slightly expanded (111) spacing (2.496Å as compared to the expected 2.431Å).[16] A weak MgO (220) peak is also observed, with a 1.506Å (near nominal) spacing. On (110) CaF_2, the strongest MgO peaks again correspond to (111) and (222), with (111) having the expanded spacing observed on (100) CaF_2. The (222) spacing has the nominal value. Peaks corresponding to (100) and (110) MgO are also observed, with intensities 20 to 33% of the (111) intensity, indicating that appreciable fractions of crystallites in the MgO film are oriented in these directions. Mismatch of (111) MgO on (100) or (110) CaF_2 is about 9%, as is (100) MgO on (110) CaF_2 and (110) MgO on (100) CaF_2, so these observed combinations are not unexpected. However, the mismatch of (110) MgO on (110) CaF_2 is 23%, so this observed orientation is unexpected.

On (111) CaF_2, the only diffraction line not attributable to the substrate

corresponds to a spacing of 3.50Å, which is not identifiable with any known spacing of MgO, MgO_2, $Mg(OH)_2$ or elemental Mg. However, this spacing is close to double the $Mg(OH)_2$ (102) spacing of 1.794Å[17] or the MgO_2 spacing of 1.700Å.[18] Thus, the formation of a magnesium oxide or hydroxide superstructure in the thin film form is a possibility on the (111) CaF_2 surface.

On SrF_2, MgO films are apparently largely amorphous to X-ray and exhibit stoichiometry problems. On (100) SrF_2, a weak MgO (111) diffraction peak occurs with the nominal 2.43Å spacing, in addition to a strong peak with a spacing of 3.22Å. This is almost exactly double the (110) spacing of elemental Mg[19] and could imply formation of a Mg superstructure. The Mg (200) line also occurs on this substrate orientation. On (110) SrF_2, the material is microcrystalline with spacings in the 4.5Å and 3.8Å regions. One weak diffraction peak at 2.266Å is attributable to α-MgF_2[12] (222, 410). On (111) SrF_2, the material is again microcrystalline with spacings in the 5.9Å region.

On CaF_2, MgO films show no variation in refractive index with substrate orientation, but different growth rates are observed. The growth rate on (100) CaF_2 is fastest, corresponding to the strongest (111) preferred orientation in the MgO film. On (110) and (111) CaF_2, growth rates are about equal and slower than on (100), corresponding to the poorer preferred orientation and formation of superstructures. On SrF_2, both growth rates and refractive indices vary with substrate orientation, greatest index and fastest growth rate occurring on (110), slowest growth and lowest index on (100), intermediate rates and index on (111). Material on (100) CaF_2 is generally crystalline while that on (110) and (111) is amorphous or microcrystalline.

Silicon Monoxide, SiO.

SiO films are non-stoichiometric, but mechanically and chemically very stable and can be used as excellent coatings for the infrared region.[7] They are nominally amorphous to X-ray and electron diffraction, but weak diffraction peaks corresponding to SiO_2 or elemental silicon are not unexpected.

On (100) CaF_2, SiO deposits with one strong tridymite (unindexed) peak with a spacing of 1.507Å.[20] No microcrystalline material is evident on this substrate orientation. On (110) CaF_2, it deposits as amorphous or microcrystalline material with spacings of the order of 1.9Å, also indicative of the tridymite phase of SiO_2[20] and of elemental silicon.[21]

On (111) CaF_2, SiO deposited as amorphous or microcrystalline material with spacings in the 1Å and 6.3Å regions in two of three cases studied. In the third case, a very strong tridymite[20] peak was observed at 3.49Å, indicating a strongly oriented, well crystallized deposit. Minor amounts of microcrystalline material with a spacing of approximately 5.9Å were also observed in this film. Growth rates of SiO are fastest on (100) CaF_2, slowest on (110), and intermediate on (111).

On SrF_2 (100), SiO films are amorphous or microcrystalline with spacings in the 1.41 and 1.46Å regions, corresponding to the tridymite phase of SiO_2.[20] On (110) SrF_2, SiO films comprise both microcrystalline and well crystallized material. Microcrystalline material has spacings in the 4Å and 2.28Å regions, corresponding to tridymite. On (111) SrF_2, SiO films show microcrystalline material in the 4 - 9Å region and the 3.7Å region, corresponding again to tridymite. Growth rates of SiO on SrF_2 are fastest on (100), intermediate on (111) and slowest on (110).

Zinc Selenide (ZnSe).

Zinc selenide crystallizes in the cubic β - ZnS structure, with space group $F\bar{4}3m$ and lattice parameter 5.668Å.[10, 22] A hexagonal form with a_o = 3.996Å and c_o = 6.53Å has also been reported, although the space group is not given, the structure is most likely similar to the α - ZnS structure.

On both (100) and (110) CaF_2, cubic ZnSe films are deposited with a strong (111) preferred orientation,[23] as indicated in tables 13 and 14. Mismatch of (111) ZnSe with (100) and (110) CaF_2 is 20% and 15%, respectively.[22] On (111) CaF_2, ZnSe is deposited in the hexagonal form with very strong (100) preferred orientation,[23] as shown in table 15. On the latter substrate, several very weak peaks attributable to $ZnSeO_4$ are also evident, as indicated in table 15. Tables 13-15 provide a fair representation of the ZnSe structure on three sets of CaF_2 substrates. Growth rates of ZnSe on CaF_2 are fastest (and essentially equal) on (100) and (110) and slowest on (111).

This growth behavior correlates very well with the structural and orientational similarities of the films on (100) and (110) and the dissimilarity on (111).

On SrF_2 substrates, the tendency toward crystallization of ZnSe in the cubic form with the (111) preferred orientation is again seen on the (100) and (110) substrate orientations. However, peaks attributable to zinc oxides, hydroxides, and selenates are also present along with broad humps in the diffractometer traces arising from microcrystalline material with spacings in the 3 to 4Å region on (110). On the (111) orientation of the SrF_2 substrates, hexagonal ZnSe is again evident, but with a weak (103) or (105) orientation (rather than (100)). In addition, large amounts

TABLE 13. Results of X-Ray Diffraction Study of $ZnSe$ on CaF_2 Substrate.

Substrate Orientation: 0° Λ (100)

Film Thickness: 10,950 Å (λ/2 at 5.3 μm)

Radiation: $Cu K_\alpha$ 35 kV. 18 mA. Ni Filter

Material	Card Ref.	Obs d (Å)	Obs I/I 100	ASTM d (Å)	ASTM I/I 100	hkl	Notes
$ZnSe$	5-0522	3.270	100	3.273	100	111	
		1.0893	<01	1.0901	08	511	
$ZnSeO_4$	19-1476	3.608	03	3.645	100	111	
CaF_2	4-0864	1.3625	08	1.366	12	400	

TABLE 14. Results of X-Ray Diffraction Study of $ZnSe$ on CaF_2 Substrate.

Substrate Orientation: 8° Λ (110)

Film Thickness: 10,950 Å (λ/2 at 5.3 μm)

Radiation: Cu K_α 35 kV. 18 mA. Ni Filter

Material	Card Ref.	Obs d (Å)	Obs I/I 100	ASTM d (Å)	ASTM I/I 100	hkl	Notes
ZnSe	5-0522	3.270	100	3.273	100	111	
		1.0893	<01	1.0901	08	511	
$ZnSeO_4$	19-1476	3.616	03	3.645	100	111	

TABLE 15. Results of X-Ray Diffraction Study of $ZnSe$ on CaF_2 Substrate.

Substrate Orientation: 1° Λ (111)

Film Thickness: 10,950 Å (λ/2 at 5.3 μm)

Radiation: CuK_α 35 kV. 18 mA. Ni Filter

Material	Card Ref.	Obs d (Å)	Obs I/I 100	ASTM d (Å)	ASTM I/I 100	hkl	Notes
Zn Se	15-105	6.50	05	----	---	001 ?	1
		3.490	100	3.43	100	100	
Zn Se O4	20-1449	4.84	03	4.94	85	011, 111	
Zn Se O4	19-1476	3.767	02	3.76	35	021	
		3.616	02	3.645	100	111	
		1.745	06	1.756	02	142	
		1.576	05	1.582	02	114	
		1.163	10	1.168	02	172, 314	
CaF_2	4-0864	3.151	>100	3.153	94	111	
		1.0515	21	1.0512	07	511	

1. d(002) = 3.25 Å; d(001) Not Listed.

of microcrystalline material with spacings in the 5-7Å region are evident on the (111) substrate orientation.

Growth rates of ZnSe on SrF_2 are fastest and about equal on (110) and (111) and slowest on (100). This behavior does not correlate well with the structural data, except for the presence of microcrystalline material on (110) and (111) and its absence on (100). This may mean that more rapid growth is associated with the formation of films having a lower degree of long range order.

Reasons for the differences in the coatings on SrF_2 and CaF_2 substrates are difficult to ascertain. Apparently, the crystal structure of the coatings on either substrate is not governed by the substrate structure or orientation for the deposition conditions employed to date. The predominant impurities on SrF_2 appear to be $Zn(OH)_2$, while those on CaF_2 appear to be $ZnSeO_4$, which may indicate the presence of small amounts of oxygen during deposition in the latter case. The hydroxide would imply the presence of water vapor in the deposition environment. These differences are not dependent on conditions in a single coating run, but represent results of at least three coating runs on each substrate material, or a total of nine samples.

Zinc Sulfide (ZnS).

Zinc sulfide crystallizes in two structures, the hexagonal α- ZnS or Wurtzite type having space group $P6_3mc$, and the cubic β - ZnS or Sphalerite type having space group $F\bar{4}3m$.[10] Both structures are based on tetrahedral coordination. In the cubic phase, zinc atoms are arranged on a face-centered cubic lattice while in the hexagonal form they fall into a distorted hexagonal close-packing. Lattice parameters

of the hexagonal phase are a_o = 3.820 Å, c = 250 Å while the cubic phase has a unit cell dimension a_o = 5.406 Å.

Alternative stacking arrangements in the c-axis direction of the hexagonal phase give rise to several polytypes of ZnS; the best known of these are designated 8H and 10H, with c-axis dimensions of 24.96 Å and 31.20 Å, respectively.[25]

On CaF_2 substrates, ZnS deposits in the hexagonal (Wurzite or α- ZnS) form, yielding diffraction patterns indicative of the 8H polytype.[25] On (100) and (110) substrate orientations the film orientation is predominantly basal with spacings of approximately 3.10 Å, or slightly smaller than the nominal 3.12 Å spacing between successive layers of Zn or S atoms.[26] The strongest diffraction peak on (100) CaF_2 corresponds to a spacing of 1.51 Å, less than half of the 3.12 Å fundamental ZnS spacing. This diffraction line is attributable to a form of α-$Zn(OH)_2$[27] with a spacing of 1.511 Å. However, the absorption results to be presented in the next section do not justify large amounts of the hydroxide material. It is thus possible that the 1.51 Å spacing corresponds to a basal ZnS spacing, considerably smaller than the nominal 1.56 Å.[24, 25] Minor diffraction lines on the (100) substrate orientation correspond to (110) ZnS(8H), at 1.905 Å, (300) ZnS (8H) at 1.102 Å, and α-$Zn(OH)_2$ (031) at 3.02 Å.

On (110) CaF_2 substrates, the situation is somewhat simpler, the strongest peak arising from the (008) spacing of ZnS (8H) at 3.11 Å. Lower intensity lines arise from (10 10), (10 13), and (110) spacings of the same material at 1.979, 1.943, and 1.887 Å (observed) and Wurtzite (102) at 2.24 Å.[024] No lines attributable to zinc oxides or hydroxides were observed.

On (111) CaF_2, ZnS again deposits in the hexagonal form with a strong preferred orientation. The strongest diffraction line corresponds to a spacing of 3.477 Å, which is very nearly three times the α - ZnS (212) spacing of 1.161 Å, also observed on these substrates. The 3.477 Å spacing does not correspond to diffraction lines for common oxides, hydroxides, sulfites, sulfates, or fluorides of zinc or to elemental zinc or sulfur. In fact, the only (non-substrate) diffraction lines observed with this substrate orientation are at 3.477 Å, 1.161 Å, and 1.06 Å, the latter attributable to α - ZnS (213). Hence we conclude that the material takes a strong preferred orientation parallel to (212), but possibly has developed a superstructure having triple the (212) spacing.

Structural mismatch criteria between the substrate and film do not appear to govern the choice of structure and orientation in these ZnS films. These criteria would predict a cubic (sphalerite or β - ZnS) structure for films on CaF_2, with a strong preferred orientation paralleling the substrate, since the structures and spacings are similar to within 1%.[24, 28] On SrF_2, these same criteria would predict α - ZnS on all three substrate orientations, with (101) ZnS paralleling (100) SrF_2, (102) ZnS on (110) SrF_2 and (100) ZnS on (111) SrF_2.[24, 29] Some of these relationships are in fact observed.

On CaF_2, the growth rate of ZnS is fastest on (110), intermediate on (100) and slowest on (111), exhibiting no obvious correlation with the structural data, except that the structure is simplest and preferred orientation strongest on (110). No extraneous lines attributable to impurities are observed on (110), but they are observed on the other substrate orientations.

Results of X-ray diffraction investigations of ZnS films on SrF_2 substrates are detailed in Tables 16, 17, and 18. On (100) SrF_2 (Table 16) the predicted very strong (101) orientation of the α - ZnS film is observed. Mismatch between film and substrate spacings in this orientation is 9.9%. On (110) SrF_2 (Table 17), the predicted (102) orientation of α- ZnS is observed. Mismatch in this orientation is 11%. Minor lines corresponding to poorly crystalline material of the 10H polytype of ZnS are also observed on this substrate orientation; none of these correspond closely to the substrate spacing.

On (111) SrF_2, the predicted (100) α - ZnS film structure and orientation are not observed (Table 18). The observed orientation of the ZnS (10H) polytype corresponds to a mismatch of approximately 10% with the substrate.[25, 29] The predicted (100) orientation of α - ZnS on (111) SrF_2 would result in a mismatch of 1.3%.[24, 29]

The growth rate of ZnS is fastest on (110) SrF_2, slowest on (100), and intermediate on (111), correlating poorly with observed structure and orientation. Slow growth of the strongly oriented, well crystallized material with low mismatch on (100) SrF_2 is quite plausible, but the rapid growth in the (102) orientation on (110) SrF_2 is difficult to reconcile with the slower growth of the 10H polytype on (111), where both have a 10% mismatch with the substrate spacing and somewhat disordered structure.

4. COATING PROPERTIES

The coating properties of interest in this study are refractive index and absorption coefficient on the various substrate materials and orientations. In order to determine these properties, single layer films of quarterwave and halfwave optical thickness at appropriate wavelengths

TABLE 16. Results of X-Ray Diffraction Study of ZnS on SrF_2 Substrate.

Substrate Orientation: 3° Λ(100)

Film Thickness: 5995 Å ($\lambda/4$ at 5.3 μm)

Radiation: Cu K_α 35 kV. 18 mA. Ni Filter

Material	Card Ref.	Obs d (Å)	Obs I/I 100	ASTM d (Å)	ASTM I/I 100	hkl	Notes
α - ZnS	5-0492	2.919	38	2.925	84	101	
		1.466	100	1.462	05	202	
SrF_2	6-0262	1.4515	80	1.4499	15	400	

TABLE 17. Results of X-Ray Diffraction Study of ZnS on SrF_2 Substrate.

Substrate Orientation: 0.8° Λ (110)

Film Thickness: 5995 Å (λ/4 at 5.3 μm)

Radiation: Cu K_α 35 kV. 18 mA. Ni Filter

Material	Card Ref.	Obs d (Å)	Obs I/I 100	ASTM d (Å)	ASTM I/I 100	hkl	Notes
α - ZnS	5-0492	2.271	100	2.273	29	102	
		1.1337	16	1.1364	<01	204	
Zn S(10H)	12-688	3.113	06	3.12	100	0 0 10	
		2.81	02	2.81	02	106	1
		2.469	01	2.49	02	--	2
SrF_2	6-0262	2.052	>100	2.0508	80	220	
		1.0253	>100	1.0253	07	440	

1. Very broad and poorly defined; microcrystalline or amorphous material.

2. The (002) spacing of elemental zinc is 2.473Å, and is thus indistinguishable from this one, within experimental error.

TABLE 18. Results of X-Ray Diffraction Study of ZnS on SrF_2 Substrate.

Substrate Orientation: 0° Λ (111)

Film Thickness: 5995 Å (λ/4 at 5.3 μm)

Radiation: Cu K_α 35 kV. 18 mA. Ni Filter

Material	Card Ref.	Obs d (Å)	Obs I/I 100	ASTM d (Å)	ASTM I/I 100	hkl	Notes
ZnS(10H)	12-688	3.6972	100	----	---	---	1
		1.8486	16	1.841	02	1 0 14	
		1.2339	13	1.239	04	ni	2
ZnS_2O_4	1-0162	~5.9	~50	5.88	100	ni	3
SrF_2	2-0262	3.336	>100	3.352	100	111	
		1.6710	86	1.6743	05	222	
		1.1149	60	1.1164	16	511	

1. Not Listed; this spacing is exactly 2 times the observed (1 0 14) spacing of ZnS(10H).

2. Other materials having similar spacings include elemental zinc (004), 1.237Å and ZnO (202), 1.238 Å.

3. Broad, poorly defined; Microcrystalline or Amorphous phase with spacing corresponding to this material.

(3.8 μm and/or 5.3 μm) were deposited on one surface of CaF_2 and/or SrF_2 substrates having nominal (100), (110), and (111) orientations.

Refractive indices were obtained from infrared transmission measurements of the quarterwave films, while absorption coefficients were measured on the halfwave films. Information on relative growth rates was obtained from spectrophotometer transmission scans of the halfwave coated samples in the visible region (600 to 800 nm), as reported in the previous section. Refractive index and absorption results are reported here, with footnotes on relative growth rates of the films added for purposes of correlation.

In order to obtain absorptance values (β and k) for halfwave thicknesses of coating materials, absorptances for the uncoated substrates must be known. The determination of the absorption coefficient of a coating material on a substrate which is transparent in the wavelength region of the irradiating laser is in principle quite straightforward. The total absorption due to a coating of specified thickness is obtained as a difference in total absorption between coated and uncoated substrates. Sequential measurements on the same substrate are utilized to obtain either a difference in absorption between coated areas or a difference in absorption in a single location before and after coating. The former method has the advantages of speed and ease of verification, but substrate inhomogeneity can cause difficulties. In the latter method, substrate inhomogeneity is eliminated, but verification of the absorption measurement on the uncoated substrate is problematic.

For an uncoated transparent substrate irradiated by a laser beam in a standard adiabatic calorimeter configuration, the total absorption A_o is given by[30]

$$A_o = \frac{2n_s}{1 + n_s^2} \qquad P_A / P_T \tag{1}$$

where n_s is refractive index of the sample, P_A is power absorbed by the sample, and P_T is the power transmitted through the sample. If the masses and heat capacities of the sample and calorimeter cone are known and irradiation times are held constant for a given series of measurements, the absorption is proportional to the ratio of output voltages from the sample and power cone thermocouples.

The total absorptance calculated from (1) includes both surface and bulk contributions. The absorption coefficient for this substrate is

$$\beta = A_o / \ell \tag{2}$$

where ℓ is the sample thickness; again, both surface and bulk contributions are included. If a coating is subsequently deposited upon such a substrate and a new absorption measurement made, the total absorptance takes on a value

$$A_t = A_o + A_1 \tag{3}$$

where A_1 is the increase in total absorptance due to the coating alone. For the case of a coating of halfwave optical thickness, A_1 can be evaluated using (1) and (3) since the surface reflectivity of the coated sample is identical to that of the uncoated substrate and the parenthetical factor involving n_s in (1) remains unchanged.

To obtain an absorption coefficient for a coating of physical thickness t_1 from a measured value of A_1, we employ a formula of Loomis,[31] with minor rearrangement,

$$\beta_1 = \frac{A_1 n_1}{2t_1 n_o} \quad \frac{(n_o + n_s)^2 \cos^2 \varphi_1 + [n_1 + (n_o n_s / n_1)]^2 \sin^2 \varphi_1}{n_1^2 + n_s^2}, \tag{4}$$

where

n_1 = film refractive index

n_s = substrate refractive index

n_o = incident medium refractive index

$\varphi_1 = 2 n_1 t_1 / o$

λ_o = laser wavelength (vacuum).

For a single coating of thickness $\lambda_o / 2$, (4) reduces to

$$\beta_1 = \frac{A_1 n_1}{2t_1 n_o} \quad \frac{(n_o + n_s)^2}{n_1^2 + n_s^2} \tag{5}$$

The absorption index of the thin film is then

$$k_1 = \frac{\lambda_o \beta_1}{4\pi} \tag{6}$$

Hence, in order to obtain the absorption coefficient and absorption index of a single layer coating on a transparent substrate, we require only the refractive index of film and substrate, the physical thickness of the film, and two absorption measurements. The method of measuring the absorption has been discussed in the literature.[32, 33]

The spectral composition of the irradiating laser has been shown to be a significant variable in absorptance measurements at CO laser

wavelengths.[14, 16] In order to verify the spectral output of both the CO and DF lasers employed in the present measurements, spectra were analyzed using a Jarrell-Ash Model 78-466 scanning spectrometer with a 50 groove/mm grating blazed at 10.0 μm and a Ge:Au detector. Spectra for the CO laser have been reported previously.[32, 34] with centroids varying from 5.25 μm to 5.45 μm, depending upon CO partial pressure. In the present study, with operating parameters typical of those employed in the calorimetric measurements (i.e. 6 mm intracavity iris, total output power ~ 2.8 W), the mean centroid of two spectra run with identical parameters was 5.29 ± .04 μm, with a bandwidth of 0.57 ± 0.1 μm.

A typical output spectrum for the CO laser is illustrated in Figure 1. Table 19 is an attempt at quantitative characterization of the spectrum. In this table, the first column gives the wavelength of individual lines as measured with the spectrometer (in air). "Line Identification" (column 2) is obtained by comparison with published data. In the third column, the mean intensity of each line is divided by that of the strongest line (7-6, P(16)), to obtain a relative intensity scale for plotting in Figure 1. The fourth column gives the mean intensity of each line divided by the summed intensity of all measured lines. The tabulated number is the fraction of laser power in any line. The fifth column, headed $|\Delta \bar{I}|$ is the standard deviation of the relative intensities from which column 3 was prepared. This is divided by the sum of intensities and tabulated in the sixth column to indicate the variability of a given line as a fraction of the laser output.

The DF laser spectrum was also analyzed in some detail since the actual output of the laser in use in the calorimetry laboratory had not been characterized previously. The same spectrometer, grating, and detector

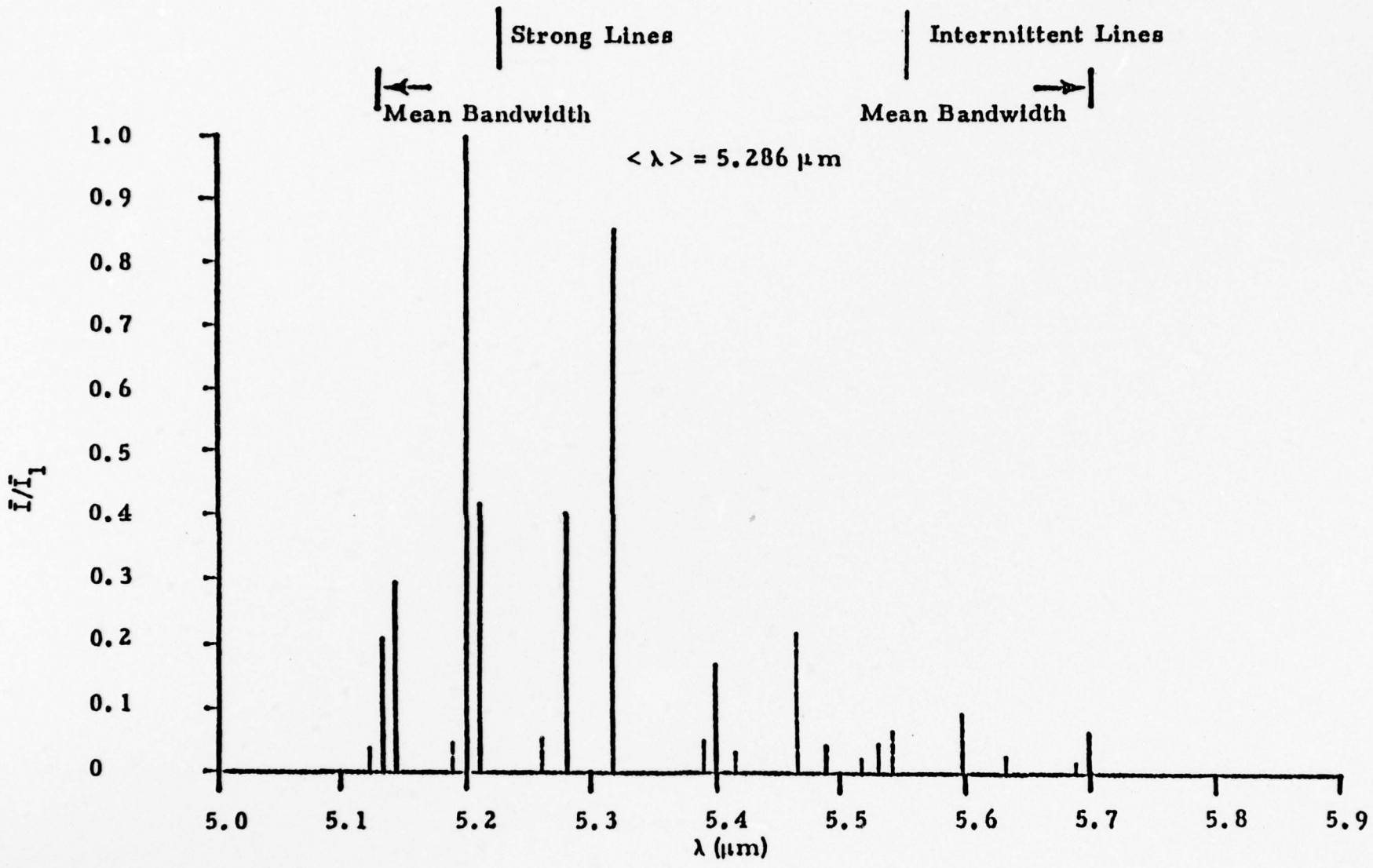


Fig. 1. Mean CO Laser Spectrum For 2 Runs With Identical Operating Parameters.

TABLE 19. Mean CO Laser Spectrum for 2 Runs with identical Operating Parameters. Mean centroid $< \lambda >$ is at 5.286 ± 0.04 μm. Mean Bandwidth is 0.57 μm. Output power is ~ 3 w, with a 6 mm diameter intracavity iris.

$\bar{\lambda}$ (μm)	Line Ident.	$\bar{I}/\bar{I}_1$	$\bar{I}/\Sigma\bar{I}$	$\lvert\Delta\bar{I}\rvert$	$\lvert\Delta\bar{I}\rvert/\Sigma\bar{I}$
5.1220	6-5, P(15)	0.037	0.009	0.052	0.012
5.1329	6-5, P(16)	0.211	0.051	0.030	0.007
5.1431	6-5, P(17)	0.292	0.070	0.071	0.017
5.1895	7-6, P(15)	0.038	0.009	0.054	0.013
5.1999	7-6, P(16)	1.000	0.240	0.000	0
5.2110	7-6, P(17)	0.420	0.101	0.303	0.073
5.2580	8-7, P(15)	0.054	0.013	0.076	0.018
5.2806	8-7, P(17)	0.412	0.099	0.112	0.027
5.3183	9-8, P(14)	0.854	0.205	0.130	0.031
5.3907	10-9, P(14)	0.050	0.012	0.071	0.017
5.40125	10-9, P(15)	0.169	0.041	0.115	0.028
5.4130	10-9, P(16)	0.031	0.007	0.044	0.011
5.4644	11-10, P(14)	0.223	0.054	0.315	0.076
5.4888	11-10, P(16)	0.043	0 010	0.061	0.015
5.5173	12-11, P(12)	0.020	0.005	0.028	0.007
5.5287	12-11, P(13)	0.044	0.011	0.063	0.015
5.5408	12-11, P(14)	0.062	0.015	0.088	0.021
5.5948	13-12, P(12)	0.090	0.022	0.127	0.030
5.6304	13-12, P(15)	0.022	0.005	0.031	0.007
5.6868	14-13, P(13)	0.012	0.003	0.0017	0.004
5.6976	14-13, P(14)	0.064	0.015	0.023	0.006
5.8394	16-15, P(12)	0.014	0.003	0.020	0.005

employed with the CO laser were used to analyze the DF. Typical operating parameters for calorimetric measurements were used. These include a helium partial pressure of ~4 Torr, with about 1.2 Torr each of SF_6 and D_2, and ~0.1 Torr of O_2 for a total of 6-8 Torr. The discharge tube is operated at a voltage of ~13 kV and current of ~450 mA to produce 2-4 W total power. Cavity temperature is ~65°C. Seven spectra were run over a three-day period and the results averaged to obtain a composite spectrum, presented in Figure 2 and Table 20.

In general, it appears that the overall spectrum is very stable with respect to centroid (~3.9 μm) and bandwidth (~0.3 μm), but individual lines are highly variable. Table 20 is an attempt at quantitative characterization of this aspect of the spectrum. In this table, the first column gives the wavelength of individual lines as measured with the spectrometer (in air). "Line Identification" (column 2) is obtained by comparison with published data.[17, 18] Column 3 ($\bar{I}$) gives the mean relative intensity of each line. The tabulated number was obtained by first determining the intensity of the line in question in each of the seven spectra, relative to the strongest line in that spectrum taken as 1.0, and then averaging the results over all seven spectra. (If a line was absent from a particular spectrum, its intensity was counted as 0.)

The mean relative intensities in column 3 of the table were divided by the sum of all of the mean intensities to obtain the fraction of the total laser energy in any given line, listed in the fourth column. The fifth column, headed "ΔI" gives the standard deviation of the mean relative intensities in column 3. This is divided by the sum of the intensities to determine the variability of a given line as a fraction of the total laser output and tabulated in the sixth column. In the seventh column, the mean relative intensity of each line is divided by that of the strongest line (2-1, P(10)), to obtain a relative intensity scale for plotting

Fig. 2 DF LASER SPECTRUM COMPILED FROM 7 RUNS OVER A 3-DAY PERIOD, OUTPUT POWER: 2-4 WATTS.

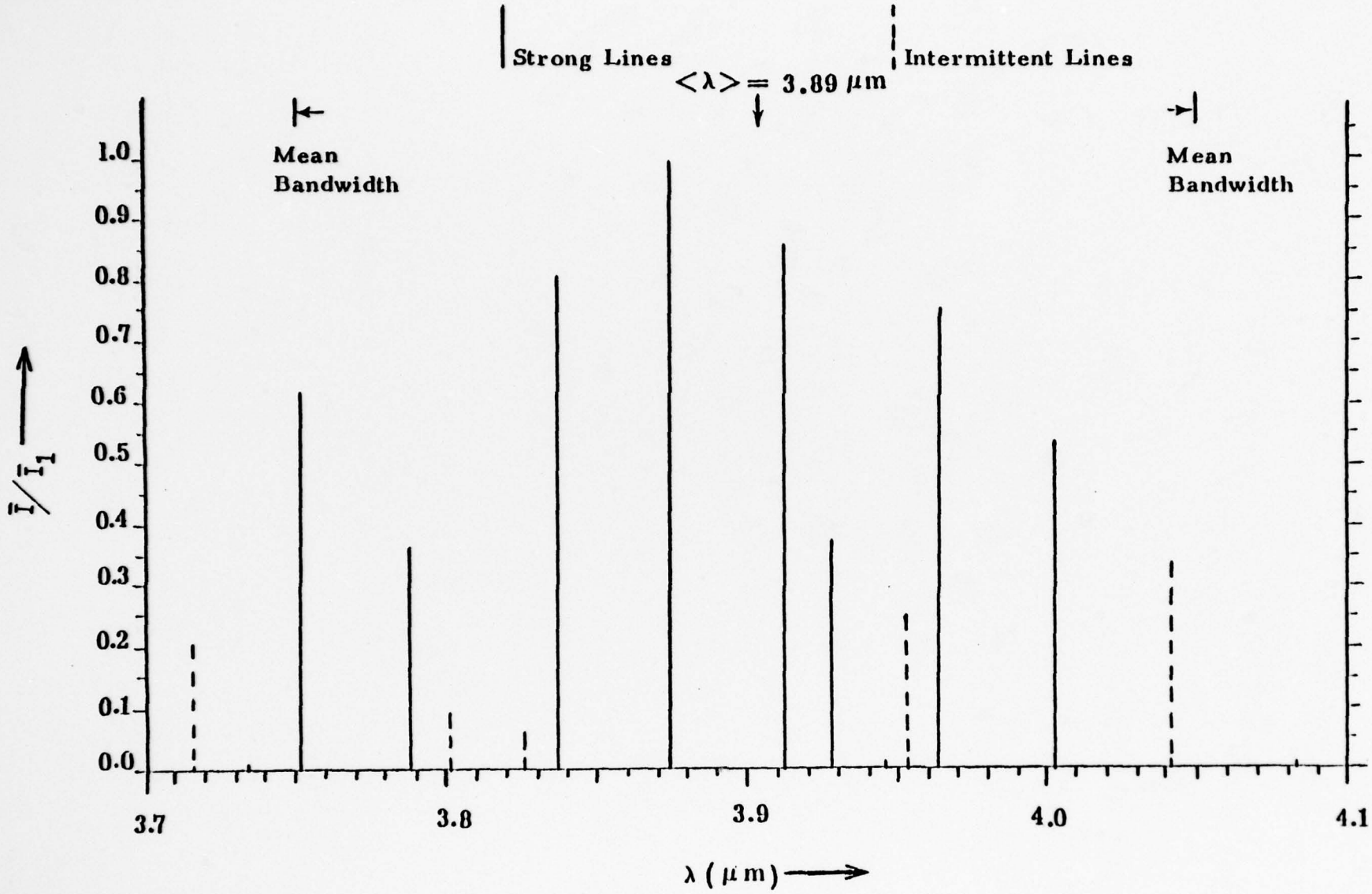


TABLE 20. DF Laser Spectrum Compiled from 7 Runs on 3 Days. Mean Centroid $\langle \lambda \rangle$ of All Spectra is 3.89 ± .025 μm. Mean Bandwidth of All Spectra is 0.297 μm ± 0.028 μm. For Individual Lines, Tabulated $\bar{\lambda}$ May Vary by ± 0.0007 μm From Run to Run.

$\bar{\lambda}$ (μm)	Line Ident.	$\bar{I}$	$\bar{I}/\Sigma\bar{I}$	$\lvert\Delta\bar{I}\rvert$	$\lvert\Delta\bar{I}\rvert/\Sigma\bar{I}$	$\bar{I}/\bar{I}_1$	No Runs Present
3.1760	1-0, P(9)	0.14	0.032	0.16	0.036	0.21	4
3.7514	1-0, P(10)	0.42	0.096	0.31	0.071	0.62	7
3.7880	1-0, P(11)	0.25	0.057	0.22	0.050	0.37	6
3.8262	1-0, P(12)	0.04	0.009	0.06	0.014	0.06	2
3.7337	2-1, P(6)	<0.01	<0.002	0.02	0.005	<0.01	1
3.8015	2-1, P(8)	0.07	0.016	0.12	0.027	0.10	2
3.8372	2-1, P(9)	0.55	0.125	0.42	0.096	0.81	7
3.8737	2-1, P(10)	0.68	0.155	0.27	0.062	1.00	7
3.9123	2-1, P(11)	0.59	0.134	0.38	0.087	0.86	7
3.9526	2-1, P(12)	0.18	0.041	0.19	0.043	0.26	4
3.9270	3-2, P(8)	0.26	0.059	0.25	0.057	0.38	5
3.9639	3-2, P(9)	0.52	0.118	0.33	0.075	0.76	7
4.0021	3-2, P(10)	0.36	0.082	0.28	0.064	0.53	6
4.0414	3-2, P(11)	0.30	0.068	0.40	0.091	0.44	4
4.0832	3-2, P(12)	<0.01	<0.002	0.02	0.005	<0.01	1
3.9457	4-3, P(5)	0.01	0.002	0.03	0.007	0.01	1

in Figure 2. Note that this number is also the fraction of total laser energy appearing in an individual line, relative to the strongest line in the composite spectrum. Finally, the last column of the table designates the number of spectra, (out of a total of 7) in which an individual line had non-zero intensity.

Results of the coating absorptance measurements carried out to date under the contract are presented in Tables 21-24, along with refractive indices determined from quarterwave films. The absorption coefficient, β, is tabulated rather than the absorption index, k, for convenience. The absorption index can of course be obtained from the β values using equation (6).

All values tabulated here differ from those presented in the previous quarterly report (May, 1977) as a result of recalculation using the program of Loomis[35] for a single layer film on the exit surface of a transparent window and correction of an error in the original calculation using equation (5).

Some general features of the data are worth noting. It appears that the coating materials fall into three broad groups, based on absorption; (1) those having β values between ~ 1 and ~ 7 cm^{-1}, (the low absorption group); (2) those having β values between ~ 9 and ~ 20 cm^{-1} (the intermediate group); and (3) those having β values of 20 cm^{-1} or more, ranging up to 100 cm^{-1} (high absorption group).

The sum of the standard deviation of the absorption measurements on the uncoated and coated substrate is a measure of the precision of the coating absorption determination. Since this determination involves the subtraction of two numbers with similar errors, the precision of

TABLE 21. ABSORPTION COEFFICIENTS OF FLUORIDE COATING MATERIALS MEASURED BY DF LASER CALORIMETRY ON COATINGS OF HALFWAVE OPTICAL THICKNESS AT A DESIGN WAVELENGTH OF 3.8 μm

COATING MATERIAL	REFRACTIVE INDEX	COATING ABSORPTION COEFFICIENT, β (cm^{-1})					
		CaF_2 SUBSTRATE			SrF_2 SUBSTRATE		
		(100)	(110)	(111)	(100)	(110)	(111)
LaF_3	1.52	41.49	28.43	24.88	36.61	24.53	29.49
MgF_2	1.36	19.06	21.70	21.17	17.56	18.33	19.20
PbF_2	1.73	4.24	3.03	7.16	2.65	5.39	4.98
SrF_2	1.34	39.81	44.71	29.24	--	--	--
ThF_4	1.49	2.86	1.65	3.58	4.43	2.76	3.59

* ON CaF_2 THE GROWTH RATE OF PbF_2 ON (110) > (111) > (100), WHILE ON SrF_2, (110) ≥ (100) > (111).

** COATINGS ON ALL SUBSTRATES EMPLOYED CERAC RAW MATERIAL. GROWTH RATES OF ThF_4 ARE INDISTINGUISHABLE ON THE THREE ORIENTATIONS OF TWO SUBSTRATE MATERIALS.

TABLE 22. ABSORPTION COEFFICIENTS OF OXIDE, SULFIDE, AND SELENIDE COATING MATERIALS MEASURED BY DF LASER CALORIMETRY ON COATINGS OF HALF-WAVE OPTICAL THICKNESS AT A DESIGN WAVELENGTH OF 3.8 μm.

COATING MATERIAL	REFRACTIVE INDEX	COATING ABSORPTION COEFFICIENT, β (cm^{-1}) CaF_2 SUBSTRATE (100)	(110)	(111)	SrF_2 SUBSTRATE (100)	(110)	(111)
Al_2O_3	1.57	40.75	37.70	29.65	45.13	43.90	32.71
MgO	1.63	65.91	86.14	79.06	62.55	100.85	102.03
SiO	1.73	2.05	2.40	2.11	3.67	5.74	2.22
ZnSe	2.42				1.08	3.73	4.69
ZnS	2.23	10.10	8.81	10.20	16.73	13.52	19.61

Al_2O_3: ON BOTH SUBSTRATE MATERIALS THE GROWTH RATE ON (100) ≅ (110) > (111).

MgO: REFRACTIVE INDEX GIVEN FOR COATINGS ON CaF_2; ON SrF_2 n(100) = 1.62, n(110) = 1.66, n(111) = 1.65. ON CaF_2, THE GROWTH RATE ON (100) > (110) ≅ (111), WHILE ON SrF_2, (110) > (111) > (100).

SiO: ON CaF_2, THE GROWTH RATE ON (100) > (111) > (110), WHILE ON SrF_2, (110) ≅ (111) > (100).

ZnSe: ON CaF_2, THE GROWTH RATE ON (100) ≅ (110) > (111), WHILE ON SrF_2, (110) ≅ (111) > (100).

ZnS: ON CaF_2, THE GROWTH RATE ON (110) > (100) > (111), WHILE ON SrF_2, (110) > (111) > (100).

TABLE 23. ABSORPTION COEFFICIENTS OF FLUORIDE COATING MATERIALS MEASURED BY CO LASER CALORIMETRY ON COATINGS OF HALFWAVE OPTICAL THICKNESS AT A DESIGN WAVELENGTH OF 5.3 μm.

COATING MATERIAL	REFRACTIVE INDEX	COATING ABSORPTION COEFFICIENT, β (cm^{-1})					
		CaF_2 SUBSTRATE			SrF_2 SUBSTRATE		
		(100)	(110)	(111)	(100)	(110)	(111)
PbF_2*	1.72	1.69	2.14	3.34	--	--	--
SrF_2	1.33	17.67	16.16	13.41	--	--	--
ThF_4**	1.48	3.24	3.11	2.98	1.41	0.78	0.78

* THE GROWTH RATE OF PbF_2 ON (110) > (111) > (110).

** COATINGS ON CaF_2 SUBSTRATES UTILIZED CERAC RAW MATERIAL; THOSE ON SrF_2 EMPLOYED BALZERS MATERIAL. GROWTH RATES ARE INDISTINGUISHABLE ON THE THREE ORIENTATIONS OF TWO SUBSTRATE MATERIALS.

TABLE 24. ABSORPTION COEFFICIENTS OF OXIDE, SELENIDE, AND SULFIDE COATING MATERIALS MEASURED BY CO LASER CALORIMETRY ON COATINGS OF HALF-WAVE OPTICAL THICKNESS AT A DESIGN WAVELENGTH OF 5.3 μm.

COATING MATERIAL	REFRACTIVE INDEX	COATING ABSORPTION COEFFICIENT, β (cm^{-1})					
		CaF_2 SUBSTRATE			SrF_2 SUBSTRATE		
		(100)	(110)	(111)	(100)	(110)	(111)
SiO	1.78	38.59	41.17	39.16	--	--	--
ZnSe	2.41	3.98	0.96	1.69	1.76	2.10	2.04
Zns	2.22	9.65	11.49	10.94	6.68	6.85	8.26

SiO: THE GROWTH RATE ON (100) > (110) ≅ (111).

ZnSe: ON CaF_2, THE GROWTH RATE ON (100) ≅ (110) > (111), WHILE ON SrF_2, (110) ≅ (111) > (100).

ZnS: ON CaF_2, THE GROWTH RATE ON (110) > (100) > (111), WHILE ON SrF_2, (110) > (111) > (100).

NORTHROP
Research and Technology Center

the results will vary. The error in the coating absorption determination for the low absorption group is of the order of 10 to 15%; that for the intermediate and high absorption groups is 3 to 5%.

In general, differences among materials are greater than differences among substrate orientations for the same coating material. However, differences among substrate orientations for the same coating may amount to factors of 2 to 4 (e.g. ZnSe on SrF_2 at 3.8 μm, Table 22, or on CaF_2 at 5.3 μm, Table 24). Structural and growth rate data are now available for establishing correlations among these properties. This will be carried out during the final phase of the effort.

5. FUTURE PLANS

The most critical tasks required to complete the contract include:

(1) βL vs. L measurements on PbF_2, ThF_4, and SiO films for halfwave, fullwave, and one and one-half wave thicknesses at 3.8 μm;

(2) Optimization of deposition conditions for ZnS and ZnSe;

(3) Deposition and characterization of AR coatings on single and polycrystalline substrates;

(4) Tests to establish the tolerance of Al_2O_3, PbF_2, ThF_4, ZnS, and ZnSe films to an HF environment.

(1), (3), and (4) have been initiated at this point in time. A first round of βL *vs.* L *measurements* has been carried out with PbF_2 films on CaF_2 (111) substrates at a design wavelength of 5.3 μm. These experiments yielded a β value of 0.26 cm^{-1} for the coating material and an absorptance of $\sim 1 \times 10^{-4}$ for the "coated surface" of the substrate.

This β is quite encouraging and the technique shows promise for isolating the absorptance of the coating material itself from that of the substrate/coating interface and the coating/air interface. Hence, we plan to carry out such measurements for three of the most promising coating materials deposited on three substrate orientations.

Three samples comprising ThF_4/SiO AR coatings on single crystal CaF_2 substrates 1.52 in. in diameter have been fabricated, characterized, and submitted to John Detrio of UDRI for damage testing. Fabrication and characterization of other designs on single and polycrystalline substrates will continue in the final phase of the effort.

REFERENCES

1. G. Hass, and E. Ritter, "Optical Film Materials and Their Applications", J. Vac. Sci. and Tech., Vol. 4, p. 71 (1966).

2. J. F. Hall and W. F. C. Ferguson, "Optical Properties of Cadmium Sulfide and Zinc Sulfide from 0.6 Microns to 14 Microns", JOSA, Vol. 45, p. 714 (1955).

3. R. J. Mattauch, "A Simple Vacuum Substrate Heater", Rev. Sci. Inst., Vol. 43, p. 148 (1972).

4. M. M. Hanson, P. E. Oberg, and C. H. Tolman, "Substrate-Temperature Measurement and Control", J. Vac. Sci. and Tech., Vol. 3, p. 277 (1966).

5. G. Hass and C. D. Salzberg, "Optical Properties of Silicon Monoxide in the Wavelength Region from 0.24 to 14.0 Microns", JOSA, Vol. 44, p. 181 (1954).

6. W. Steckelmacher, in Thin Film Microelectronics, L. Holland, Editor, p. 193, John Wiley & Sons, Inc., New York (1965).

7. K. H. Behrndt, in Physics of Thin Films, G. Hass and R. E. Thun, Editors, Vol. 3, p. 1, Academic Press, New York (1966).

8. L. Holland, Vacuum Deposition of Thin Films, Chap. 3, Chapman and Hall, London (1956).

9. R. W. G. Wyckoff, Crystal Structures, 2nd ed. Vol. 2, Wiley, N.Y. (1964).

10. R. W. G. Wyckoff, Crystal Structures, 2nd ed. Vol. 1, Wiley, N.Y. (1963).

11. ASTM Powder Diffraction File: Card No. 6-0290.

12. ASTM Powder Diffraction File: Card No. 16-160.

13. S. J. Holmes and P. Kraatz, "Investigation of Crystal Orientation Influence on Thin Film Coatings for CaF_2 Laser Windows" AFML Technical Report TR-75-188, Air Force Materials Laboratory, Wright-Patterson Air Force Base, Ohio 45433, (1965).

REFERENCES (cont'd)

14. ASTM Powder Diffraction File Card Nos. 23-1423 and 23-1426.

15. M. O. Aboelfotoh, K. C. Park, and W. A. Pliskin, "Infrared and high-energy electron diffraction analyses of electron-beam-evaporated MgO films" J. Appl. Phys. V. 48, pp. 2910-2917, 1977.

16. ASTM Powder Diffraction File Card No. 4-0829

17. " " " " " No. 7-239

18. " " " " " No. 19-771

19. " " " " " No. 4-0770

20. ASTM Powder Diffraction File Card Nos. 18-1170, 14-260.

21. " " " " " No. 5-0565

22. " " " " " No. 5-0522

23. " " " " " No. 15-105

24. " " " " " Nos. 5-492, 5-566.

25. " " " " " No. 12-688

26. A. R. Verma and P. Krishna, "Polymorphism and Polytypism in Crystals" Wiley, NY, 1966.

27. ASTM Powder Diffraction File Card No. 20-1437.

28. " " " " " No. 4-0864.

29. " " " " " No. 6-0262.

30. R. Weil, "Calculations of Small Absorption Coefficients From Calorimetric Experimental Data", Appl. Phys., Vol. 41, p. 3012, (1970).

31. J. S. Loomis, "Absorption in Coated Laser Windows", Appl. Opt. Vol. 12, p. 877, (1973).

32. P. Kraatz, and P. J. Mendoza, "CO Laser Calorimetry for Surface and Coating Evaluation", Proc. Fourth Conf. on Infrared Laser Window Materials, p. 77, (1975).

33. T. F. Deutsch, "Research in Optical Materials and Structures for High Power Lasers", Final Technical Report, Raytheon Research Division, ARPA Order 1180 (1973).

34. Kraatz, P., Holmes, S. J., and Klugman, A., "Absorptance of Coated Alkaline Earth Fluoride Windows at CO Laser Wavelengths", Proc. Fifth Conf. on IR Laser Window Materials, DARPA, (1975).

35. Loomis, J. S., "Computing the Optical Properties of Multilayer Coatings", Air Force Weapons Laboratory Technical Report No. AFWL-TR-75-202, September, 1975.